TEKNILLINEN KORKEAKOULU
Faculty of Electronics, Communications and Automation
Department of Automation and Systems Technology

LULEÅ
UNIVERSITY
OF TECHNOLOGY

Jan Philipp Hakenberg

Mobility and Autonomous Reconfiguration of Marsokhod

A Thesis Submitted
in Partial Fulfillment of the
Requirements for the Degree

Master of Science in Technology

Supervisors:

Professor Aarne Halme
Helsinki University of Technology

Professor Kalevi Hyyppä
Luleå University of Technology

Instructor:

Mikko Elomaa
Helsinki University of Technology

Espoo, August 2008

Helsinki University of Technology — Abstract of the Master's Thesis

Author:	Jan Philipp Hakenberg
Title of the thesis:	Mobility and Autonomous Reconfiguration of Marsokhod
Date:	August 2008 — **Number of pages:** 58
Faculty:	Electronics, Communications and Automation
Department:	Automation and Systems Technology
Program:	Master's Degree Program in Space Science and Technology
Professorship:	Automation Technology (Aut-84)
Supervisors:	Professor Aarne Halme (Helsinki University of Technology)
	Professor Kalevi Hyyppä (Luleå University of Technology)
Instructor:	Mikko Elomaa (Helsinki University of Technology)

We investigate the mobility of Marsokhod onto which we have installed new hardware. We introduce backlash compensation for the arm joints, and wheel control with a continuous duty cycle. Calibration of the wheels allows us to measure the load on the wheels accurately.

The robot responds autonomously to the level of the supply voltage, the information of the accelerometer, and the load on the wheels. The overall performance is a smooth superposition of individual behaviours. Our control software has a simple interface. An operator commands the robot to conduct advanced motions with only a joystick.

Keywords: automation, autonomous reconfiguration, Marsokhod, Mars rover, mobility, optimal control, robotics

Acknowledgment

I thank Mikko Elomaa for his consultation on the electronics as well as his support to conduct the field experiments. As my instructor, he has kindly tolerated my slightly off-topic, time-consuming explorations.

My research is partially funded by a grant from the European Space Agency ESA.

I express my gratitude to 王翰康, Michal Hoč, and 永井将貴. All students of the Erasmus mundus course made the stay and studies joyful – thank you all!

I am grateful to my family, who supported me by keeping me up to date on what's going on at home. The trilogy is complete.

Contents

Symbols and abbreviations

x	robot coordinates
$\mathbf{U}$	supply voltage with motors stopped
U	supply voltage
$\mathbf{w}$	angular no load speed
$\mathbf{r}$	wheel radius
$\mathbf{i}$	inclination of wheel blades
$\mathbf{y}$	base-line of the yaw rate gyroscope
$\mathbf{a}$	distance from joint to exterior axle
$\mathbf{b}$	distance from center axle to joint
c	clearance between center and exterior axle
α	elevation of joint
θ	tilt between center and exterior axle
$\mathbf{h}$	period of one communication cycle
idt	identifier tag
con	period of clock, and period of velocity estimation
icr	period of pulse width modulation
pwm	duty cycle of motor
drv	desired direction of motor
eim	update stp on measured direction change
tim	clock
enc	count of encoder, revolution of motor
stp	enc at last measured direction change
dir	measured direction of motor
vel	angular velocity of motor
d	duty cycle of motor
t	time of mission
$\bar{p}$	position of motor
$\bar{w}$	velocity of motor
lcd	character on LCD
led	state of LED
dog	dead man's switch

yaw	rotational rate around x_3
acc	accelation
tlt	tilt between exterior and center axle
vcc	supply voltage
ω_3	rotational rate around x_3
a	acceleration
$\bar{b}$	measured backlash of the wheel and joint bearings
b	measured backlash of the joint bearings
P, $P^{\pm}$	functions to incorporate the backlash
p	position of wheel or joint
w	velocity of wheel or joint
ζ	scale factor of motor
W	function mapping duty cycle to no load velocity
$\hat{w}$	no load velocity of wheel or joint
ν	estimated no load velocity of wheel or joint
δ	coefficients for estimation
l	load, velocity defect
ξ, Ξ	coefficients for estimation
τ	torque
m	elementary motion
$\hat{F}$	function of turning efficiency
n	compensatory motion
ρ	placement of axles
v	velocity of motion
ϱ	intended direction of driving
κ	truncation factor
Υ	voltage drop
$p_{\min}$	lower bound of inclination
$p_{\max}$	upper bound of inclination
v_{d}	target velocity
h^{v}, h^{s}	velocity distribution
CAN	controller area network
LAN	local area network
ASCII	american standard code for information interchange

Chapter 1

Introduction

Marsokhod is a vehicle developed by the Mobile Vehicle Engineering Institute VNIITRANS-MASH in St. Petersburg, Russia. The 6-wheeled, skid steered rover with wheel walking capability was intended to maneuvre on Mars in 1997. Eventually, the Mars-96 mission by the Russian Space Agency did not incorporate the robot [Za96].

Instead, the rover was employed for simulations on planetary exploration conducted at several cross country locations around Earth as listed in Figure 2.1. The rover served as a platform to carry scientific loads. Tests emphasized aspects such as imaging systems, vision-based navigation, and remote control. None of the well-documented missions have challenged the extensive terrain capabilities of the rover. Nevertheless, [CW97] and [SC01] report on problems in precise navigation. The experience gained from these early tests must have influenced the design and operation of the Mars rovers Sojourner, Spirit and Opportunity.

Several publications discuss the mobility of Marsokhod, however, the researchers have neglected the inclination of the wheel blades [AA98], and [PL03]. On weak grounds, the configuration of the blades greatly enhances the turning efficiency. The inclination of the blades is indicated in (3.1).

Typically, the literature conceives wheel walking in the context of cresting steep, sandy mounds. The bending of the joints alters the clearance between the axles. When maneuvring on a course with obstacles of up to the size of a wheel, the adaptive placement of the axles is another great benefit of the articulated joints.

The Marsokhod at the Automation Technology Laboratory of the Helsinki University of Technology is at an early stage of development, see Figure 3.4. The undercarriage is equipped with strong motors, high-resolution optical encoders, and electronics for control. The configuration allows to put the mobility of the robot to the test, and to research on suitable driving parameters.

We derive wheel velocities to accompany the bending of the articulated joints. The sus-

Figure 1.1: Left: Snow wraps around the wheels. Plastic foil shields the onboard computer from moisture. Right: “Such a rover has practically no road clearance.” [Ke90].

pension of the axles changes inclination, which the motors are required to compensate. Moreover, we model the backlash of the joints for smooth wheel walking. Our efforts culminate in developing an autonomous reconfiguration that enhances safety and performance of the robot.

The convenient interface to our system that drives the robot is intended for operator control, and future application software, see Figure 3.9. Our solutions are inspired by field experiments, that we carry out in the vicinity of the laboratory. Video clips of all field experiments are featured on [Ha08]. Since every outside run helps to improve at least one aspect of the system, we perform numerous of these experiments beginning with

Field Experiment 1.1 (28. Mar 2008)**.** Marsokhod was operated in the car park of the department. A layer of snow as well as artificial humps of snow covered the asphalt. The rover was powered and commanded through a tether, see Figure 1.1.

The snow wrapped quickly around the wheels impairing the mobility of the robot. Wheel walking helped Marsokhod to overcome the piles of snow; the joints levered the robot away from humps. Two times during the run, the rear joint motion was not correctly tracked. Later on, investigations revealed a loose connection at the motor encoder in the rear joint. □

Several concepts that we project on Marsokhod have proven their value in a simulated or theoretical environment beforehand: The position and velocity control for the joints was tested in a computer game [Ha04]. The methodology of superimposing elementary motions to yield advanced movement is common in mathematics. When working with robots, we follow the guidelines

- ◊ respect the hardware
- ◊ value sensor accuracy
- ◊ centralize the information
- ◊ fuse sensors only when unmistakable
- ◊ ensure analyzable control
- ◊ rule out stupid robot behavior

Now, let us outline the content of the Thesis: Chapter 1 summarizes the history of Marsokhod. We state the intentions of the inventors. We recap the field experiments related to planetary exploration conducted on behalf of the National Aeronautics and Space Administration NASA.

In Chapter 2, we turn towards the Marsokhod rover that was aquired by the Helsinki University of Technology. Close inspection of the electronics motivates significant modifications to the circuitry. We summarize the final design: the list of components added as well as the physical quantities relevant to the operation and mobility of the robot. Since we program the controllers that operate the motors, and that read out the sensors, we explain the interface to the controllers.

The procedures and results established in Chapter 3 prepare Marsokhod for the operation in the field. The rear joint of Marsokhod exhibits considerable backlash that we incorporate in our model for hassle-free bending of the joints. We calibrate the wheels, and investigate the load response. We present the position control for smooth and precise joint inclination. Tests show that the type of control is suitable for wheel walking.

Some fundamental questions remain until this point: How does Marsokhod turn in the most efficient manner? What are the correct motor velocities during wheel walking? Chapter 4 gives answers. Additionally, the most common wheel walking patterns are listed. The patterns are incorporated into our software and are approved in the field.

In Chapter 5, we present the driving support system, that is inspired from and validated in the operation of Marsokhod in the field: The use of a simple mathematical relation prevents a voltage drop below a certain threshold while navigating, thus improves operational stability. The control of the joints involves several degrees of freedom, such as the upper and lower bound of the inclination. We explain reasonable autonomous modifications to these parameters based on the sensor measurements. To enhance traction, the power of slipping wheels is distributed to wheels with better grip.

Finally, we conclude and summarize the contributions of the thesis. We make suggestions for the future development of Marsokhod.

Chapter 2

Background

An early prototype of Marsokhod existed in 1990, see Figure 2.2. Research on the robot was active during the following decade due to the interest in the exploration of Mars. The science institutes referred below purchased the robot from VNIITRANSMASH, which is the exclusive manufacturer of the chassis.

Our emphasis is on the mobility and autonomous reconfiguration of Marsokhod. We give direct quotes to preserve the nuances of the authors. For instance, Quote 2.2 relates the configuration of the chassis and wheel walking mode to the external circumstances as listed in the early paper [KG92].

2.1 Mobile Vehicle Engineering Institute

Marsokhod was designed to navigate on the surface of Mars [KG92]. The leading engineer, A. Kermurjian, explains the intentions behind the remarkable layout in

Quote 2.1. from [Ke90], *Modern Concept of the Marsokhod*: "The greatest cross-country capability can be ensured if the rover is a wheel-walker with a three-part configuration and a hinged frame. Such a rover has practically no road clearance. This is achieved by using conical wheels that provide a continuous support surface for the rover, thus ensuring a cross-country capability for terrains full of obstacles and ruling out the rover's getting stuck on a high center obstacle. The hinged frame and a special drive for folding or raising the sections enable it to overcome obstacles whose height is twice the wheels' diameter."

The *Small Marsokhod Configuration* has the following characteristics: The ground track is of variable length 70–170 cm, and fixed width 70 cm. The wheel radius is 17.5 cm. Motors, batteries, and scientific apparatus are to be installed inside the conical wheels for a low center of mass.

In 1993, initial tests in Kamchatka, Russia, tested the virtual reality remote control of the robot and imagers. The engineers claim that the robot could climb a slope of granular soil

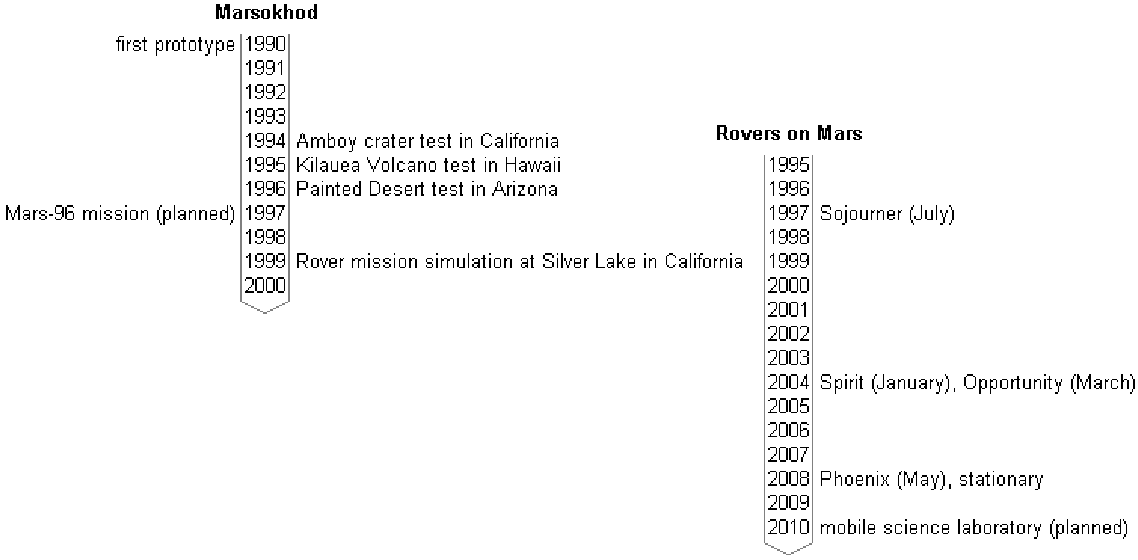

Figure 2.1: Left: History of Marsokhod. Right: Rovers on Mars listed with month of arrival.

with inclination of 20 deg while driving, but overcome an ascent of 25–30 deg using wheel walking [KG92].

The next quote gives the reason for our interest in autonomous reconfiguration that we develop in Chapter 6.

Quote 2.2. from [KG92], p. 167: "The combining in switching the wheel drives and the frame mechanics provides the implementation of several motion modes.

MODE	CONDITIONS
Wheel mode of motion:	
with minimum base	Areas with accumulations of stones, slightly rugged terrain. Maneovring under hindered conditions. Turning on weak grounds
with nominal base	Principal mode of motion on mean rugged terrain
with increased base	Benches, slopes. Increase in course stability
with forced bending of frame	Overcoming of high obstacles. Hanging of motor wheels which failed
Wheel walking mode of motion	Considerable lifts on granular grounds, including maximum equal to angle of repose of ground (30–35 degrees). Dangerous obstacles and their combinations
Wheel walking mode of motion with forced reconfiguring of frame	Overcoming of fractures, accumulations of stones

This constructional design allows to solve the problems on ripping-up of the surface ground layer by means of the wheels, which in practice is impossible for the movers of other types."

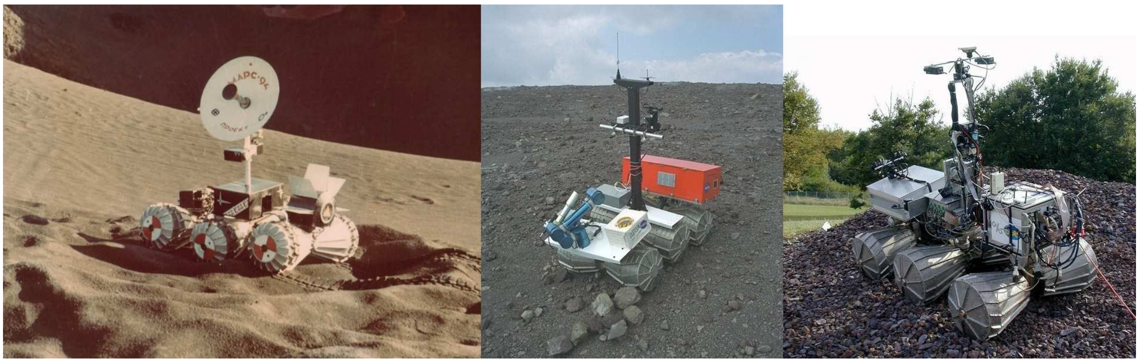

Figure 2.2: Left: “Prototype rover with conical wheels”, reproduced from [Ke90]. Center: Marsokhod at Silver Lake, reproduced from [SC01]. Right: Marsokhod at the Laboratoire d’Analyse et d’Architecture des Systèmes, reproduced from [La08].

2.2 Ames Research Center

During the period 1994–1996, the NASA Ames Research Center employed Marsokhod as the undercarriage in several field experiments that would support the upcoming Mars Pathfinder mission and the Sojourner rover. Due to the size of Marsokhod, no miniaturization was needed to test relevant field experiments. The objectives of the first three field trials are summarized in [CW97]:

The Amboy crater test in California emulated significant time delays, and placed emphasis on the interaction of the remote science team. The Kilauea Volcano test in Hawaii added a manipulator to the vehicle, and increased the variety of control.

The objective of the test in the Painted Desert region of Arizona was to establish the general geology and biology of the site. The location featured sparse vegetation, diverse geology, and had a Mars-like appearance. Marsokhod carried an instrument and sampling arm, imaging systems, onboard computers, vision-based navigation, and a remote control interface. Fully equipped, the robot weighed about 100 kg. The rover was powered through a tether.

Subsequently in 1999, Marsokhod served as the mobile platform in the field experiment held near Silver Lake in the Mojave Desert [SC01]. The experiment simulated the operational environment and the science data returned by a Mars rover. The simulation inspired future Mars missions, when there was the opportunity to investigate the geologic and climate history with possibly life and water.

Essential parts of the equipment were a color stereo imager, a visible near-infrared fiberoptic spectrometer, an infrared spectroradiometer, and several monochrome cameras for the localization and navigation algorithm. A robotic arm was to excavate a trench into the subsurface and to take close-up pictures. The weight of the robot had increased to 120 kg.

The researchers investigated the effectiveness of imagery and spectroscopy of the rover platform. Images of subsurface materials at a microscopic scale were available from digging conducted below the surface. The team of scientists experienced both the capabilities as well as the limitations of the mission, and their feedback was able to improve operational procedures. Algorithms for onboard data analysis were tested.

Quote 2.3. from [SC01], Section 3: "The rover was navigated using one of two modes. In the first mode, called *dead reckoning*, the rover was simply commanded to turn to a given heading relative to the current heading and then move a certain distance in that direction. The second navigational mode used a vision-based tracking system to autonomously drive the robot to a natural feature (e.g., a rock outcropping) designated by the operator. The target object is kept in view by the rover's mast camera as the rover moves toward it."

The authors reported that the navigation of Marsokhod is limited to only a few meters per command cycle. A sequence of commands positioned Marsokhod accurately. The authors recommendation was for improvement of the onboard autonomy.

2.3 Laboratoire d'Analyse et d'Architecture des Systèmes

Engineers at the Laboratoire d'Analyse et d'Architecture des Systèmes near Toulouse, France, have used the Marsokhod platform for testing sensors and algorithms in the field between 1996 and 2002. The activities and results are summarized in [La08]. The researchers refer to Marsokhod as Lama.

In the first stage, the robot is equipped with a magnetic fluxgate compass, two-axes inclinometer, and optical encoders. Two Motorola 68k microprocessors control the rover motion, and collect the sensor data. A stereo bench is mounted on top of a mast, and the images are processed in an onboard computer. The rover is supplied by 26 V batteries located inside the wheels. According to the model of robot-soil interaction in [AA98], wheel walking increases the slope coverage from 25 to 30 deg.

Subsequently, a second stereo bench is mounted on the front axle of Marsokhod, and a fiber-optic gyrometer replaces the compass. A conventional GPS qualifies the localization algorithms developed at the laboratory. Fully equipped, the robot weighs about 180 kg, see Figure 2.2. Henceforth, navigation and mapping techniques are tested. Videos available online suggest that the robot does not drive forward and turn at the same time. [La08] states the maximum speed as 0.17 m/s.

The final locomotion control is summarized in [PL03]. The wheel speeds for turning are derived geometrically, however, the inclination of the blades is neglected. The experiments that we carry out in Section 5.1 reveal a simple criteria to turn Marsokhod efficiently: The wheels of the center axle should not slip, but bear as much load as possible.

The researchers model ground traction according to three states listed in the quotation below. In Section 6.3, we introduce a method that responds to slippage in a continous fashion.

Quote 2.4. from [PL03], Section IV: "Many experiments were made with Lama, with situations among 3 main categories, corresponding to 3 states: State 0: Easy situation for the rover. It seems that there is no abnormal slippages. State 1: Difficult situation for the rover. Some abnormal slippages happen, but the robot is still moving forward. State 2: Locomotion Fault. Because of excessive slippages the rover does no longer move forward, even though its wheels keep on turning."

2.4 Automation Technology Laboratory

The Helsinki University of Technology, Finland, purchased a Marsokhod rover for educational purposes. Students have installed H-bridges, controller boards, and a PC104 to the robot. The efforts are reflected in their theses that were submitted in 2007:

Jason Allan designed an energy management system for Marsokhod with NiMH-batteries placed inside the wheels. The MAX712 chip conducts Delta-V recharging.

Zhongliang Hu applied the Ziegler-Nichols method to derive the coefficients of the PID-velocity control of the wheels. Driving tests including wheel walking were carried out.

Poornima Muralidhar proposed to drive Marsokhod along curves parameterized by Bézier[1]-polynomials. Software was developed to simulate a sequence of maneuvres.

Prior to our work, the robot comprised of the hardware listed below.

	NUM	ID
Fabrimex DC-DC converter, 9–39 V to 5 V, 5 A max.	1	ECW24–0525
Ampro computer, Intel 650 MHz Celeron processor	1	ReadyBoard 710
Arcom CAN interface, 8-bit PC104 module	1	AIM104-CAN
AT90CAN128 header board with JTAG connector	8	AVR-H128CAN
CAN physical layer transceiver	8	SN65HVD230
Maxon RE 36, DC motor, ∅36 mm, graphite brushes, 70 W	8	118798
Maxon Planetary Gearhead GP 42 C, ∅42 mm, 1:230 ratio	8	203131
Maxon Encoder HEDS 5540, 500 counts per turn, 3 channels	8	110513
LSI quadrature clock converter	8	LS7184

The various power supplies to Marsokhod are

POWER SUPPLY	ID
Velleman DC Power Supply, 0–30 V, 2×2.5 A	PS 613
HUANYU rechargeable battery, 2×12 V, lead-acid, 5 Ah	HYS1250
HUANYU rechargeable battery, 2×12 V, lead-acid, 4 Ah	HYS1240

[1]Pierre Étienne Bézier, * 1. Sep 1910 in Paris, † 25. Nov 1999

Figure 2.3: Photos from [TK08]. Left: Marsokhod on a platform at the Helsinki University of Technology. Right: *WorkPartner in the park.*

That the Marsokhod was given to us operational in principle has greatly facilitated the undertakings of this Thesis. We were granted a convenient starting point to test the subsystems and to fine-tune the interplay between the components. In Section 3.1, we motivate the modifications of the electronics that we make.

Another reconfigurable robot at the laboratory is WorkPartner. [Le07] implements autonomous reconfiguration for WorkPartner to enhance and simplify the operation. The robot switches state according to sensor measurements.

Quote 2.5. from [Le07], Section 6.4: "The mode changes to rolking occurred at the right moment when WorkPartner encountered vertical obstacles, when the wheel started to slip a lot or energy consumption increased due to soft soil. The mode changes happened before WorkPartner damaged the soil a lot. It also changed to wheeled mode when the terrain was traversable for wheels; furthermore, only a very small amount of needless mode changes occurred."

A finite state machine brings difficulties:

Quote 2.6. from [Le07], Section 7.2: "The effect of driving speed on the automatic locomotion mode control should be studied further. A time window is needed for preventing unnecessary mode change, because values of criteria may briefly exceed thresholds at times and lead to unnecessary mode change. Scaling the time window with respect to the speed of the robot should be studied further in wheeled mode."

The autonomous reconfiguration that we design for Marsokhod is a continous superposition of behaviours and does not require switching between states. Moreover, the bending of the joints at arbitrary rates and amplitudes – wheel walking in general – is superimposed over ordinary driving and turning.

Chapter 3

Implementation

The central processing unit of Marsokhod is the ReadyBoard with an Intel Celeron chip running at 650 MHz. The operating system is Debian GNU/Linux, kernel 2.6.8. The computer processes all the measurements of the sensors on the robot, and devises the control over the motors. For monitoring and hi-level control, the ReadyBoard communicates to the outside world via a wireless LAN interface as sketched in Figure 3.4.

There are 9 controllers $\mu_0, \mu_1, \ldots, \mu_8$ of type AT90CAN128 onboard of Marsokhod. The operating voltage is 5 V. For proper operation at 16 MHz, the fuse bytes are set as

EXTENDED	HIGH	LOW
`0xFF`	`0x19`	`0xCF`

The communication lines of the controllers are connected star-like to the CAN interface, a PC104 module mounted on the ReadyBoard. A resistor of 123 Ω at the CAN interface terminates `CANH` and `CANL`.

Information is passed via the CAN bus at 1000 kbit/s. The CAN messages consist of an 11-bit identifier tag idt and data of up to 8 bytes. In our implementation, we assign the 8 highest bits of idt only, while the lowest 3 bits are always zero.

[At08] is the primary reference to program the controllers. [Po07] explains how to address the CAN interface mounted on the ReadyBoard.

3.1 Adjustments and final specifications

To investigate the hardware of the robot, we utilize

INSTRUMENT	ID
Hewlett Packard Oscilloscope, 60 MHz	54603B
Hewlett Packard Function/Arbitrary Waveform Generator, 15 MHz	33120A
Voltcraft Digital Multimeter, principle tolerance 0.8%	VC-160

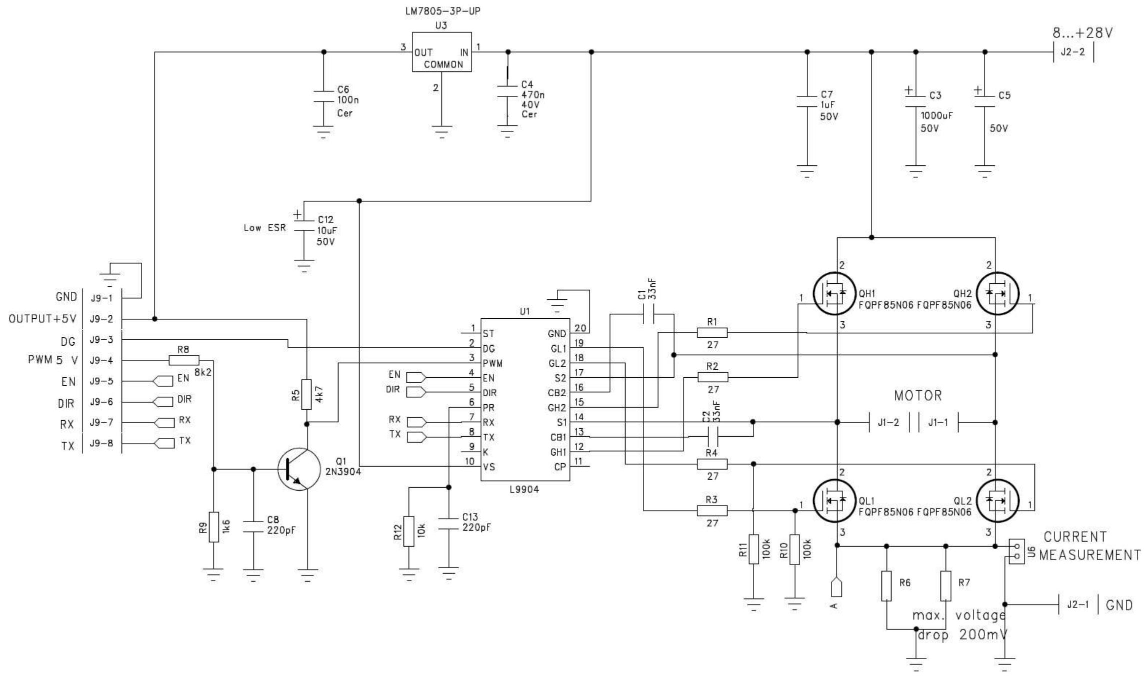

Figure 3.1: Schematics by Kalle Rosenblad; H-bridge with driver installed to Marsokhod.

Results from early tests have suggested modifications of the electronics as well as the software on the controllers and the ReadyBoard:

The Fabrimex DC-DC converter is not suitable for longterm operation of all the 5 V appliances on Marsokhod. However, the converter has excellent noise characteristics. We install a separate Finlandia Interface DC-DC converter to power the ReadyBoard. The overall power consumption remains invariant.

Cables for communication to the controllers inside the rear wheels were torn during a nominal wheel walking procedure. The new cables that we install are more flexible. Now, the cables to supply the H-bridges are 16×0.2 mm windings, consistently.

The H-bridge designed by Kalle Rosenblad, an engineer at the laboratory, has a superior performance over the H-bridge previously installed to Marsokhod [Ha08]. We equip Marsokhod with the new circuits displayed in Figure 3.1.

The pin `OC1A` of the AT90CAN128 outputs the duty cycle to the H-bridge, but does not perform correctly at any of the controller boards. Instead, we assign `OC1B` to the H-bridge driver.

The pin `CLK` of the clock converter LS7184 cannot catch up to the pulses of the encoders, due to the resistor value at `RBIAS` [LS07]. Instead of replacing the resistor, however, we simply route the encoder output to `T3` of the controller.

Previously, resistors of 120 Ω between `CANH` and `CANL` at all CAN transceivers resulted in a total resistance of just 13 Ω between the bus lines. The CAN interface on the ReadyBoard has a terminating resistor of 123 Ω. Since the controllers are connected in a starlike fashion

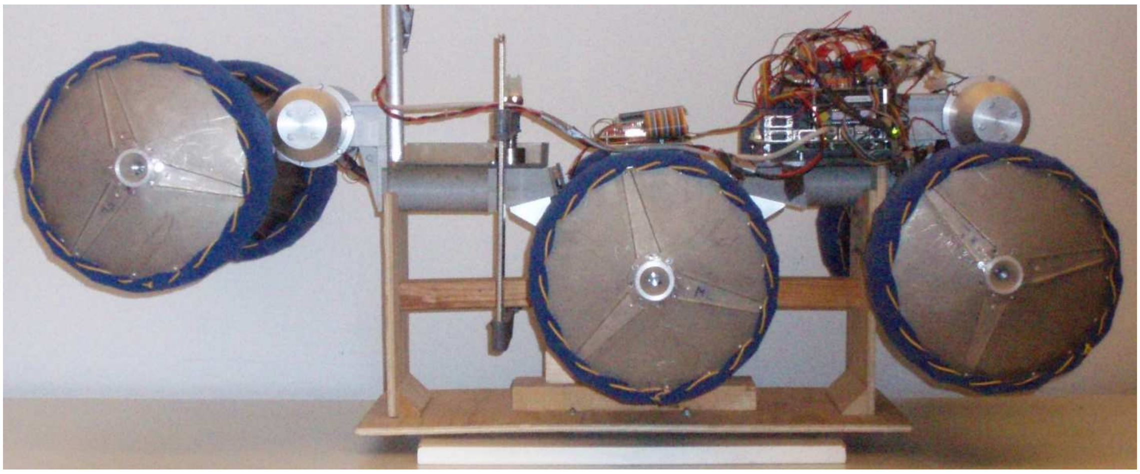

Figure 3.2: Marsokhod on the maintenance socket. The front joint is extended.

to the module, we remove the resistors at the CAN transceivers.

The old controller software truncated the resolution of the encoder pulses by a factor of 2. Our new code cherishes sensor accuracy.

Previously, a CAN data bus rate of 250 kbit/s was used. We increase this rate to the maximum of 1 Mbit/s.

We contribute the following hardware to Marsokhod:

	NUM	ID
protective cover for the wheel, blue carpet, width 15 cm	6	
Finlandia Interface DC-DC conv., 10–39 V to 5 V, 10 A max.	1	SR902500-5-M
D-Link Wireless network adapter, USB	1	DWL-G122
AT90CAN128 header board with JTAG connector	1	AVR-H128CAN
CAN physical layer transceiver	1	PCA82C250
H-bridge, driver L9904, max. frequency 30 kHz	8	
3-axis accelerometer, range ± 14.7 m/s^2, analog signal	1	MMA7260Q
$\pm 300°$/s yaw rate gyroscope with SPI	1	ADIS16100
Voltage divider, 24 V to 4.44 V	1	
LCD with driver, 16 characters	1	TM161A/B
LED, in series with a 50 Ω resistor	2	

With the protective covers strapped to the wheels, driving Marsokhod inside the laboratory is harmless to the floors. The covers are made from robust carpet. Due to the configuration of the sharp blades, the slip between the wheel and the cover is negligable. A protective cover is strapped tight by knotting a single ribbon. Consequently, the cover is removed with the same ease. Figures 3.2 and 4.7 display the robot with protective covers on.

Section 3.3 addresses the new sensors, the LCD, and the LEDs. When an external torque inhibits a wheel from turning, the power consumption is high and the supply voltage drops.

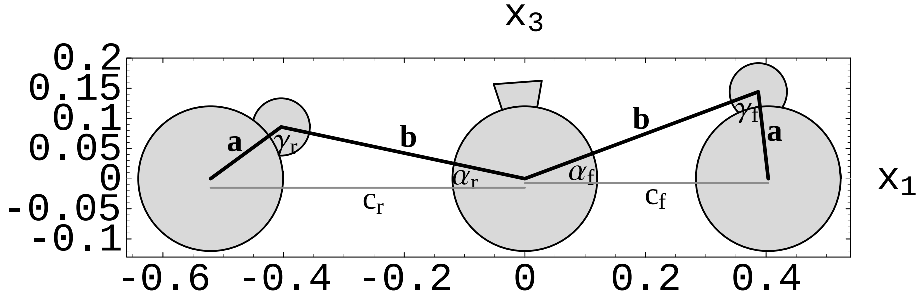

Figure 3.3: Geometric variables relevant to the mobility of the robot. The central unit is tilted by $\frac{1}{2}(\alpha_f - \alpha_r)$. The drawing is true to scale, the unit is meter.

The measurement of the supply voltage enables us to drive Marsokhod more safely.

We summarize the specifications relevant to our research.

	VAR	MIN	TYP	MAX	UNIT
supply voltage with motors stopped	$\mathbf{U}$		24	27	V
supply voltage	U	20	24	27	V
encoder pulses per revolution of shaft			115000		
angular no load speed	$\mathbf{w}$	-2.827		2.827	rad/s
wheel radius	$\mathbf{r}$	0.115		0.125	m
inclination of wheel blades	$\mathbf{i}$		0.240		rad
base-line of the yaw rate gyroscope	$\mathbf{y}$	490	505	520	
distance from joint to exterior axle	$\mathbf{a}$		0.145		m
distance from center axle to joint	$\mathbf{b}$		0.413		m
clearance between center and exterior axle	c	0.333		0.550	m
elevation of joint	α	0		0.359	rad
tilt between center and exterior axle	θ	-0.524	0	0.524	rad
period of one communication cycle	$\mathbf{h}$		0.016	0.032	s

During driving phase the supply voltage drops $\mathbf{U} - U > 0$, which is related to the motor control and load as stated in (4.5). According to the field experiments, a battery voltage below $U < 20$ V might cause the computer to reboot.

Several geometric variables are visualized in the figure above. On solid terrain, the blades contribute to the wheel radius $\mathbf{r}$, whereas $\mathbf{r} = 0.115$ on granules. The Maxon RE 36 datasheet states the maximum angular speed at 24 V as 2.8274 rad/s. Procedure 4.5 shows how the no load speed increases while the motors warm up.

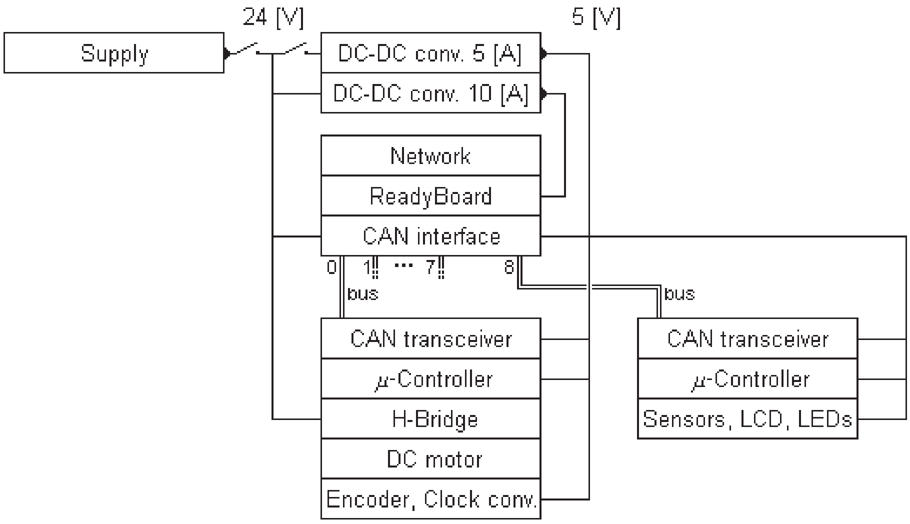

Figure 3.4: Power supply and functional arrangement of the electronic appliances.

At $U = 24$ V, the current consumption of the stationary Marsokhod composes of

DEVICES	MIN	UNIT
converter 10 A max., ReadyBoard, PC104 modules	0.69	A
H-bridges, CAN interface	0.13	A
converter 5 A max., controllers, encoders, analog sensors	0.23	A

During heavy duty driving, the current flow might exceed 5 A.

We remark on our nomenclature. The data related to the 8 motors of Marsokhod is arranged in matrices of the form

$$\begin{bmatrix} \mathsf{BL}, 4 & & \mathsf{CL}, 2 & & \mathsf{FL}, 0 \\ & \mathsf{AB}, 7 & & \mathsf{AF}, 6 & \\ \mathsf{BR}, 5 & & \mathsf{CR}, 3 & & \mathsf{FR}, 1 \end{bmatrix} \rightarrow$$

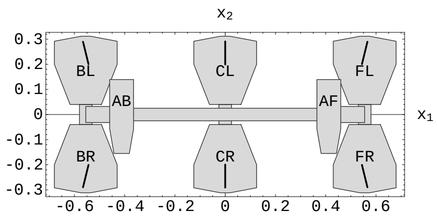

(3.1)

FL abbreviates *front-left* wheel, and so forth. The digits enumerate the wheels and joints. For instance, w_3 is the velocity of the right wheel of the center axle. p_7 is the inclination of the rear joint. The coordinate x_3 counts upwards. The point $(0, 0, 0)$ is located at the center of the center axle. The drawing is true to scale, the unit is meter.

3.2 Motor tracking and control

The AT90CAN128 chips $\mu_0, \mu_1, \ldots, \mu_7$ each control a single H-bridge with motor. The controllers are arranged as

$$\begin{bmatrix} \mu_4 & & \mu_2 & & \mu_0 \\ & \mu_7 & & \mu_6 & \\ \mu_5 & & \mu_3 & & \mu_1 \end{bmatrix}$$

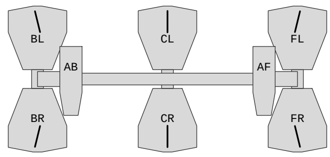

using the notation (3.1). For instance, μ_6 is assigned to the front joint. The controller μ_i for $i = 0, 1, \ldots, 7$ manages the state of the motor i by defining the duty cycle at a certain modulation frequency. The controller also tracks the encoder pulses and the measured motor direction.

The input variables to μ_i for $i = 0, 1, \ldots, 7$ are

VAR	MIN	TYP	MAX		CONVERSION	UNIT
con	0	1	255	period of clock, and period of velocity estimation	$(\mathsf{con} + 1)\frac{65536}{2000000}$	s
icr	255	511	2047	period of pulse width modulation	$(\mathsf{icr} + 1)\frac{1}{8000000}$	s
pwm	0		icr	duty cycle of motor	$(-1)^{\mathsf{drv}}\mathsf{pwm}/\mathsf{icr}$	
drv	0		1	desired direction of motor	$0 = \circlearrowleft$, $1 = \circlearrowright$	
eim	0		1	update stp on measured direction change	1=enabled	

The symbol $\circlearrowleft$ denotes counter-clockwise around the x_2-axis. For instance, to drive the robot forward, we set $\mathsf{drv} = 0$ for all wheels.

The controller μ_i outputs the variables

VAR	BITS		CONVERSION	UNIT
tim	16	clock	$\mathsf{tim}\frac{\mathsf{con}+1}{2000000}$	s
enc	16	count of encoder, revolution of motor	$\mathsf{enc}\frac{2\pi}{115000}$	rad
stp	16	enc at last measured direction change	$\mathsf{stp}\frac{2\pi}{115000}$	rad
dir	1	measured direction of motor	$0 = \circlearrowleft$, $1 = \circlearrowright$	
vel	15	angular velocity of motor	$\mathsf{vel}\frac{25\pi}{47104(\mathsf{con}+1)}$	rad/s

The communication is initiated by the ReadyBoard. Any request sent by the ReadyBoard targets a unique controller μ_i for $i = 0, 1, \ldots, 7$, which responds thereupon. The highest 4 bits of the identifier tag idt specify the destination i, the subsequent 4 bits specify the type of the request. The lowest 3 bits of idt are zero.

Typically, the period of one communication cycle is $\mathbf{h} = 0.0156$ s, which corresponds to a frequency of 64 Hz.

Control: The 3 byte request of the frame sets the duty cycle, while the 8 byte response encodes real-time, motor position, and velocity.

	idt	0	1	2	3	4	5	6	7
REQUEST	0xi0	drv,eim	$\mathsf{pwm}_{\mathrm{h}}$	$\mathsf{pwm}_{\mathrm{l}}$					
RESPONSE	0xi1	$\mathsf{tim}_{\mathrm{h}}$	$\mathsf{tim}_{\mathrm{l}}$	$\mathsf{enc}_{\mathrm{h}}$	$\mathsf{enc}_{\mathrm{l}}$	$\mathsf{stp}_{\mathrm{h}}$	$\mathsf{stp}_{\mathrm{l}}$	$\mathsf{dir},\mathsf{vel}_{\mathrm{h}}$	$\mathsf{vel}_{\mathrm{l}}$

The value pwm determines the torque of the motor in the direction specified by drv. The duty cycle is

$$d = (-1)^{\mathsf{drv}} \frac{\mathsf{pwm}}{\mathsf{icr}}$$

pwm should not exceed icr, so that $d \in [-1, 1]$. Two consecutive requests should not differ significantly in pwm. The bit drv should only toggle, when pwm is close or equal to zero. d^k for $k = 0, 1, 2, \ldots$ denotes the sequence of duty cycles. Any significant difference $|d^k - d^{k-1}|$ causes a peak consumption in current, and needless stress on the motor.

Due to the characteristics of the clock converter LS7184, we set the bit

$$\mathsf{eim} = \begin{cases} 1 & \text{if } \mathsf{pwm}/\mathsf{icr}{<}0.6 \\ 0 & \text{otherwise} \end{cases}$$

The response retrieves the status of the chip and the encoders. The controller μ_i has a 16-bit clock that overflows every

$$T(\mathsf{con}) = \frac{\mathsf{con} + 1}{2000000} 65536 \text{ [s]}$$

If the period of one communication cycle $\mathbf{h}$ is below $T(\mathsf{con})$, we reconstruct the time of transmission t^k by

$$t^k = t^{k-1} + \frac{\mathsf{con} + 1}{2000000} (\mathsf{tim}^k - \mathsf{tim}^{k-1})_{\mathrm{mod}\ 65536} \text{ [s]} \tag{3.2}$$

The variable con determines the period of the clock, as well as the velocity estimation. con is selected so that $T(\mathsf{con})$ exceeds the duration of one communication cycle $\mathbf{h} < T(\mathsf{con})$. Otherwise, the overflows of tim, and thus the time of transmission t, are not tracked correctly by (3.2).

The variable enc counts the pulses by the encoder independent of the direction of the motor. The value overflows at 65536, which corresponds to a revolution of 102.6 deg. The angular position of the motor accumulates as

$$\bar{p}^k = \bar{p}^{k-1} + (-1)^{\mathsf{dir}^{k-1}} \frac{2\pi}{115000} \begin{cases} (\mathsf{enc}^k - \mathsf{enc}^{k-1})_{\mathrm{mod}\ 65536} & \text{if } \mathsf{dir}^k = \mathsf{dir}^{k-1} \\ (\mathsf{stp}^k - \mathsf{enc}^{k-1} - \mathsf{enc}^k + \mathsf{stp}^k)_{\mathrm{mod}\ 65536} & \text{otherwise} \end{cases}$$

in rad.

Remark 3.1. Typically, we initialize the robot with the joints vertical and set

$$\bar{p}^0 = \begin{bmatrix} 0 & & 0 & & 0 \\ & 1.2121 & & -1.2121 & \\ 0 & & 0 & & 0 \end{bmatrix}$$

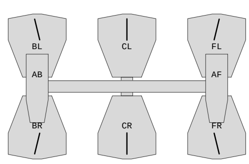

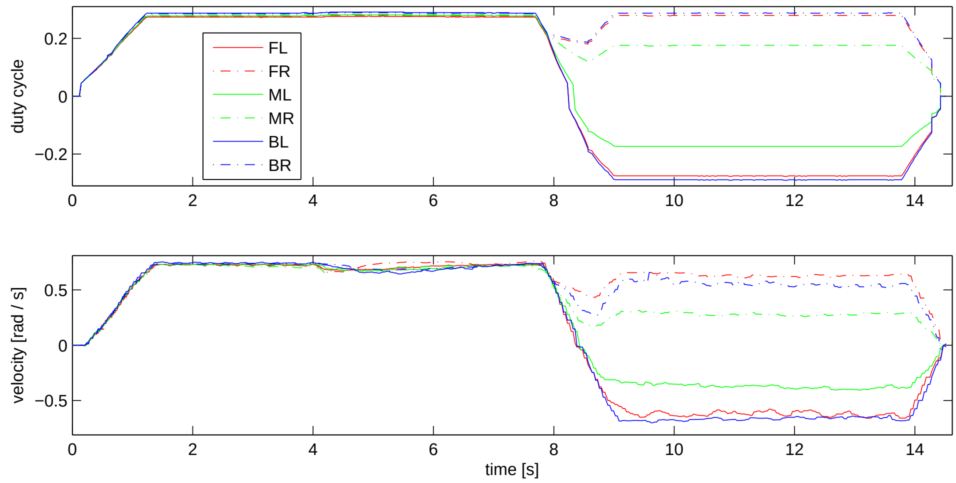

Figure 3.5: Maneuvre of driving forward followed by turning on the spot. Between 4–7 s, the front-left wheel of Marsokhod overcomes an obstacle. The joints are at rest and not displayed. Top: Duty cycles d_i for $i = 0, 1, \ldots, 5$. Bottom: Motor speeds $\bar{w}_i$ measured by the optical encoders.

The value $\arccos \mathbf{a}/\mathbf{b} = 1.2121$ rad corresponds to the angles γ_f, γ_r. Recall from Section 3.1, that $\mathbf{a} = 0.145$ m, and $\mathbf{b} = 0.413$ m. □

The instantaneous angular velocity of the motor is

$$\bar{w}^k = (-1)^{\mathsf{dir}^k} \frac{25\pi}{47104(\mathsf{con}+1)} \mathsf{vel} \text{ [rad/s]} \tag{3.3}$$

The value vel is simply the number of encoder pulses that occured during one period T. Due to the maximum angular speed of about $\mathbf{w} = 2.827$ rad/s, the value of vel ranges from 0 to $\lceil 1727.27(\mathsf{con}+1) \rceil$. The velocity is positive when the motor shaft rotates counter-clockwise around the axis x_2.

Figure 3.5 relates the input to the output in a standard driving situation.

Configuration: The modulation frequency to the motors as well as the period of velocity estimation typically remain constant during a single driving phase. The two parameters icr, and con are configured for initialization and only sporadic during operation.

	idt	0	1	2	3	4
REQUEST	0xi2	icr_h	icr_l	pwm_h	pwm_l	con
RESPONSE	0xi3	tim_h	tim_l			

The value icr defines the period of the pulse-width modulated duty cycle as $\frac{1}{8000000}(\mathsf{icr}+1)$ s. For instance, $\mathsf{icr} = 511$ corresponds to a frequency of 15.625 kHz. Because icr is not buffered in the controller during update, icr should only be modified when pwm is close or equal to zero.

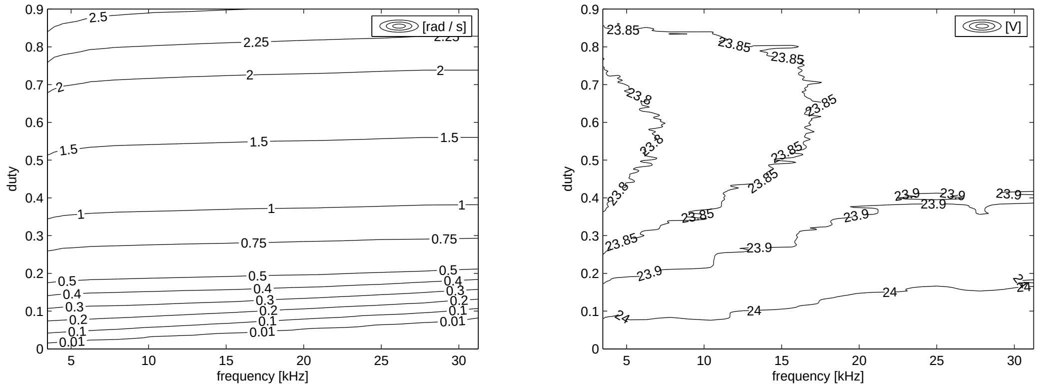

Figure 3.6: No load motor velocity at different modulation frequencies. The voltage drop is proportial to the power consumption of the motor.

Remark 3.2. Values of icr above a threshold (about $600 \leq$ icr) result in unpleasant sound induced by the motor while pwm $\neq 0$.

Generally, an increase of icr raises the current consumption of the motor. However, the motor is more resistant to load and can be assigned lower speeds.

Lowering the value of icr reduces the current consumption of the motor while driving at low load. On the other hand, load slows the motor down easily, and at small values of pwm the motor might stop suddenly. ☐

Figure 3.6 visualizes the motor response in the no load situation at different operating frequencies. In Section 4.3, we investigate the load response further. Due to the subtleties remarked, we fix icr $= 511$ as a simple compromise.

The controllers $\mu_0, \mu_1, \ldots, \mu_7$ have identical pin assignments:

PIN			VAR
8	`T3`	external timer counter to register the rising edges of the encoder logic pulses	enc
15	`OC1A`	(defective)	
16	`OC1B`	pulse-width modulated signal with frequency below 31.25 kHz duty cycle of motor	pwm
25	`INT0`	external interrupt on rising and falling edge in case of direction change of motor	dir
30	`TXCAN`	transmit bits to CAN transceiver	
31	`RXCAN`	receive bits from CAN transceiver	
37	`PC2`	desired direction of motor	drv

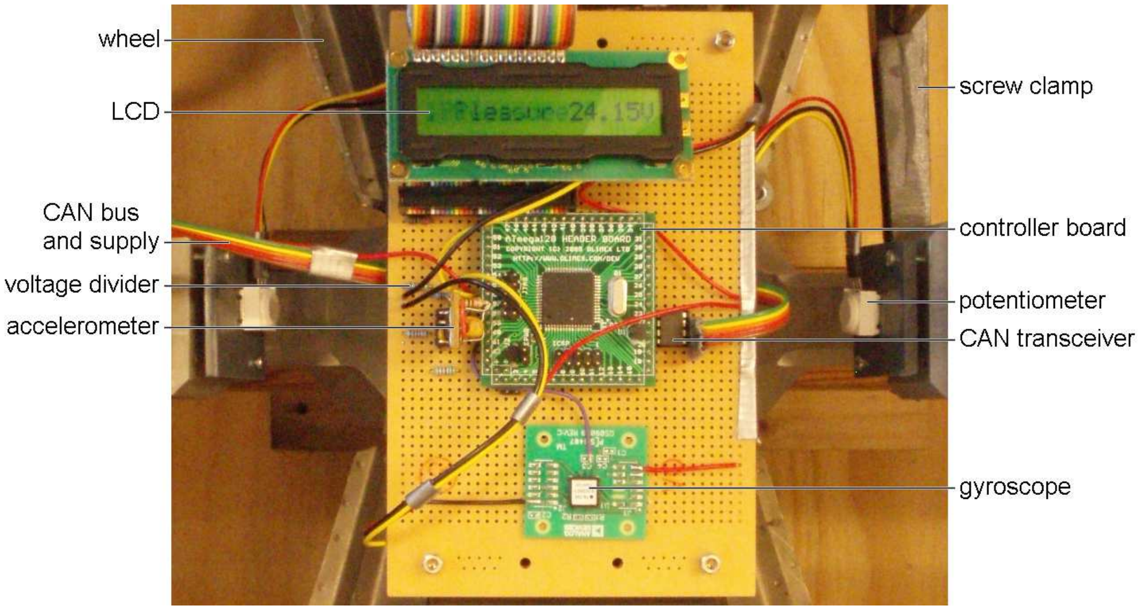

Figure 3.7: Photograph of μ_8 with sensors, while Marsokhod is clamped to the maintenance socket. When the CAN bus is inactive, the LCD displays the text "Pleasure in the job puts perfection in the work." The LEDs are not shown in the photograph.

3.3 Basic measurements

The controller μ_8 measures seven analog signals: A resonator gyroscope measures the rotational rate around x_3. A 3-axes accelerometer gives information about the slant of Marsokhod. A potentiometer measures the inclination of the front axle with respect to the center axle. Another potentiometer measures the inclination of the rear axle with respect to the center axle. A voltage divider breaks down the present supply voltage U, which varies depending on the driving load and on the type of supply.

The controller displays the supply voltage as well as text specified by the application software on a 16-character LCD. The display informs the operator on the state of the batteries. The controller also switches two bright LEDs: led^0 emits green light, while led^1 shines in white.

The input to controller μ_8 is

VAR	MIN	MAX		CONVERSION	UNIT
lcd^i	32	127	character $i = 0, 1, \ldots, 7$ on LCD	ASCII	
led^i	0	1	state of LED $i = 0, 1$	$0 =$ off, $1 =$ on	
dog	0	255	dead man's switch ($0 =$disable)	$\mathsf{dog}\frac{65536}{250000}$	s

The output provided by μ_8 is

VAR	TYP		CONVERSION	UNIT
yaw	$\mathbf{y}$	rotational rate around x_3	$0.0170(\mathbf{y} - \mathsf{yaw})$	rad/s
acc^1	279	accelation along x_1	$0.0732\,\mathsf{acc}^1 - 20.42$	m/s^2
acc^2	251	accelation along x_2	$0.0746\,\mathsf{acc}^2 - 18.76$	m/s^2
acc^3	376	accelation along x_3	$0.0652\,\mathsf{acc}^3 - 14.69$	m/s^2
tlt^f	527	tilt between front and center axle	$+0.00495\,\mathsf{tlt}^f - 2.61$	rad
tlt^r	520	tilt between rear and center axle	$-0.00526\,\mathsf{tlt}^r + 2.74$	rad
vcc	970	supply voltage	$0.0677\,\mathsf{vcc} - 41.08$	V

The TYP values are recorded for Marsokhod at rest on a flat ground on Earth with the joints equally inclined. Figure 3.8 illustrates the conversion of the readings into physical units.

Measurements: The data of the CAN messages in one communication cycle between the ReadyBoard and μ_8 is

	idt	0	1	2	3	4	5	6	7
REQUEST	0x80	$\mathsf{led}^0, \mathsf{lcd}^0$	$\mathsf{led}^1, \mathsf{lcd}^1$	lcd^2	lcd^3	lcd^4	lcd^5	lcd^6	lcd^7
RESPONSE	0x81	yaw_h	$\mathsf{acc}^1_\mathrm{h}$	$\mathsf{acc}^2_\mathrm{h}$	$\mathsf{acc}^3_\mathrm{h}$	tlt_h	vcc_h	b_6	b_7

The bit led^i for $i = 0, 1$ refers to the highest bit. The ASCII character lcd^i for $i = 0, 1, \ldots, 7$ is assigned the 7 low bits. b_6 refers to the concatenation of the two lowest bits of $\mathsf{yaw}, \mathsf{acc}^1, \mathsf{acc}^2$, and acc^3. b_7 holds the two lowest bits of tlt, and vcc. The lowest bit j of b_7 informs whether tlt corresponds to tlt^f when $j = 0$, or tlt^r when $j = 1$. The bit j alternates after one communication cycle.

Resonator gyroscopes as the ADIS16100 on Marsokhod are sensitive to temperature. Moreover, the measurements typically drift within a window of 5 LSB at a rate no greater than 0.01 LSB/s. We compensate the bias offset using a simple strategy: Whenever Marsokhod is not in motion, we estimate the null rate reading $\mathbf{y}$ using the low-pass filter $\mathbf{y}^{k+1} = \lambda \mathbf{y}^k + (1 - \lambda)\mathsf{yaw}^k$ for a coefficient λ close to 1. While driving, we set $\mathbf{y}^{k+1} = \mathbf{y}^k$. The rotational rate of Marsokhod around x_3 is

$$\omega_3 = 0.0170(\mathbf{y}^k - \mathsf{yaw})\,\mathrm{rad/s} \tag{3.4}$$

The conversion factor 0.0170 corresponds to room temperature.

The accelerometer MMA7260Q operates in the range of ± 14.7 m/s^2 for each of the 3 axes. However, the sensor has been in use for over 3 years, which might explain why the three axes exhibit different characteristics. We calibrate the sensor in

Procedure 3.3. We let the accelerometer come to rest with one axis $i = 1, 2, 3$ parallel to gravity. Depending on the direction, acc^i attains either the minimum or the maximum. The value by the analog-to-digital converter acc represents $\pm g = 9.81$ m/s^2.

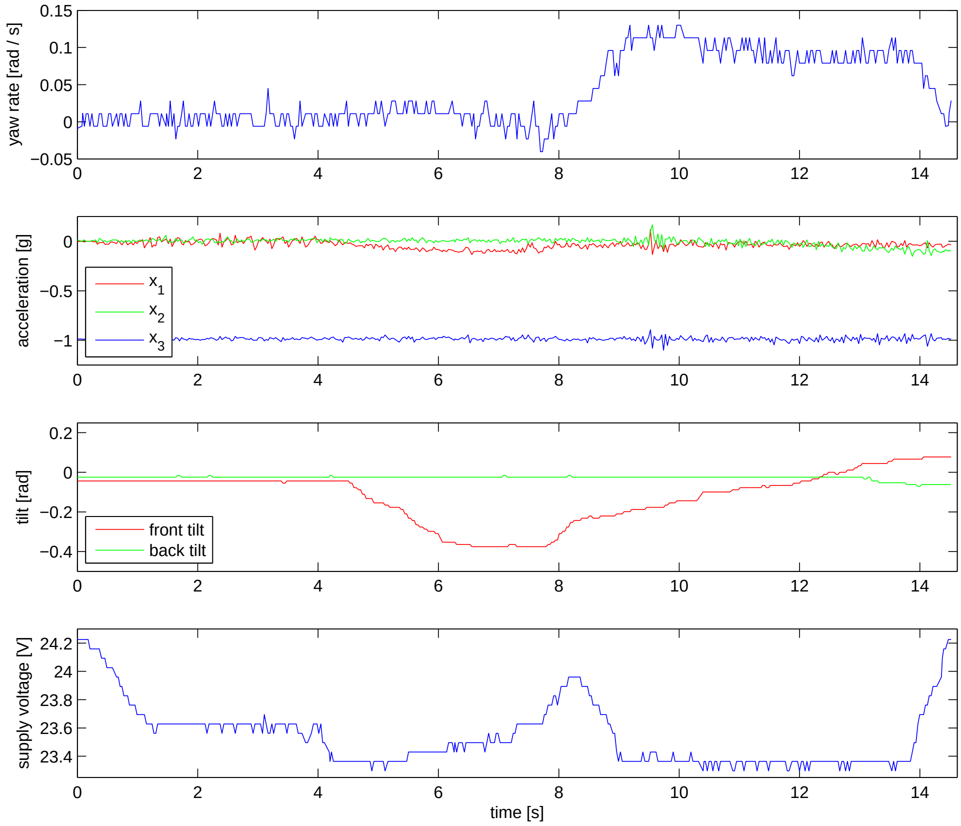

Figure 3.8: Sensor measurements during the maneuvre displayed in Figure 3.5. The gyroscope indicates the turning during 8–14.5 s. The obstacle causes a voltage drop between 4–7 s.

CHANNEL	$-g$	g
acc^1	145	413
acc^2	120	383
acc^3	75	376

Using linear interpolation, the acceleration is

$$a^i_{\mathsf{acc}} = 9.81 \frac{\mathsf{acc}^i(g) + \mathsf{acc}^i(-g) - 2\,\mathsf{acc}^i}{\mathsf{acc}^i(g) - \mathsf{acc}^i(-g)} \,\mathrm{m/s}^2 \tag{3.5}$$

for $i = 1, 2, 3$ in the coordinate system of the accelerometer. □

In Subsection 6.2.1, we estimate the slope of the terrain from a_{acc}, accounting also for the configuration of the joints.

Procedure 3.4. We tilt the front and rear axles with respect to the center axle. The potentiometers shown in Figure 3.7 vary resistance accordingly. The readings at the limit of ± 30 deg are linearly interpolated, similar to (3.5). The formulas that convert tlt^f and tlt^r into θ_f, and θ_r are

$$\theta_f = +0.00495\,\mathsf{tlt}^f - 2.61 \text{ rad}$$
$$\theta_r = -0.00526\,\mathsf{tlt}^r - 2.74 \text{ rad}$$

The backlash of the potentiometers affect the measurements. The error is about ± 8 deg. □

In our model, we neglect θ_f, and θ_r.

The nominal supply voltage of 24 V is broken down by a voltage divider of 300 kΩ and 68.1 kΩ to 4.44 V at pin `ADC6` of μ_8. While the robot is in motion, the voltage U typically drops by several 100 mV, which in turn affects the performance of the motors.

Procedure 3.5. We record the analog-to-digital conversion of `ADC6` at several supply voltages U ranging from 27 down to 20 V, which is characteristic for battery operation.

U is measured by a multimeter at the power distribution board on Marsokhod, while the chip outputs $\mathsf{vcc} \in [0, 1023]$. The affine linear relation with the least squared error is $U = 0.06768\,\mathsf{vcc} - 41.0823$ V. Due to the 10-bit resolution of the analog-to-digital conversion, the error is below ± 34 mV. □

Let U^k be the measured supply voltage in iteration k. To estimate the reference voltage $\mathbf{U}$, we define the sequence

$$\mathbf{U}^{k+1} = \begin{cases} \max(U^k, \lambda \mathbf{U}^k + (1-\lambda) U^k) & \text{if } d_i^k = 0 \text{ for all motors } i = 0, 1, \ldots, 7 \\ \max(U^k, \mathbf{U}^k) & \text{otherwise} \end{cases}$$

with $\mathbf{U}^0 = U^0$ and a coefficient λ close to 1. The formula ensures $U \leq \mathbf{U}$.

Fuse: The controller μ_8 can act as a dead man's switch. The safety measure is disabled by default.

	idt	0
REQUEST	0x82	dog
RESPONSE	0x83	

The dead man's switch is disabled when $\mathsf{dog} = 0$. If $\mathsf{dog} > 0$, the μ_8 stops the motors $0.2621\,\mathsf{dog}$ seconds after the last arrival of a message with $\mathsf{idt} = \mathtt{0x80}$. μ_8 stops the motors by sending CAN messages with $\mathsf{idt} = \mathtt{0xi0}$ for $i = 0, 1, \ldots, 7$, that set $\mathsf{pwm}_i = 0$.

We summarize the connections of controller μ_8.

PIN			VAR
5	PE3	white LED with pull-up resistor	led^1
15	OC1A	(defective)	
16	PB6	green LED with pull-down resistor	led^0
30	TXCAN	transmit bits to CAN transceiver	
31	RXCAN	receive bits from CAN transceiver	
44	PA7	LCD upper 4-bit of bidirectional tri-state bus	
45	PA6		
46	PA5		
47	PA4		
49	PA2	LCD enable line, operation start signal for data	
50	PA1	LCD read/write line	
51	PA0	LCD select line	
55	ADC6	supply voltage U broken down by a voltage divider	vcc
56	ADC5	tilt of back axle with respect to middle axle	tlt^r
57	ADC4	tilt of front axle with respect to middle axle	tlt^f
58	ADC3	acceleration along x_3	acc^3
59	ADC2	acceleration along x_2	acc^2
60	ADC1	acceleration along x_1	acc^1
61	ADC0	rotational rate around x_3	yaw

The coordinate axes are with respect to the sensors. Let Marsokhod be at rest on a flat ground with the joints equally inclined, i.e. $\alpha_f = \alpha_r$ in Figure 3.3. Then, the coordinates of the sensors are identical to the coordinates of the robot as layout in (3.1).

3.4 Software architecture

Besides the software for the controller, we develop the C program *Mediator* that addresses the CAN interface of the ReadyBoard. The program polls for incoming TCP network messages from a client that contain the low-level control of the controllers. *Mediator* decomposes the information, and forwards the commands to the individual controllers. The replies by the controllers are concatenated into a single TCP packet, and routed back to the client.

The Java program *Joyride* is the client software to *Mediator*. *Joyride* is either located on the ReadyBoard, or on another PC. For efficient development, we devise and test the control algorithms from a Desktop PC, but during the field experiments *Joyride* is hosted on the ReadyBoard. Low-level motor control via a wireless link is not safe, since the connection might stall and leave the motors in their current state.

Joyride converts high-level control, such as driving forward, turning, and bending the

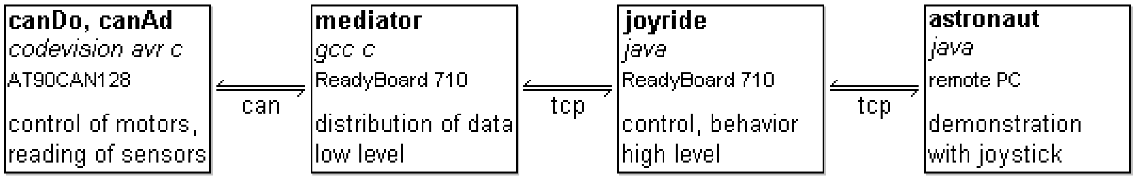

Figure 3.9: Final software architecture to drive Marsokhod.

joints, into appropriate motor control that is forwarded to *Mediator*. When the network connection to the ReadyBoard is interrupted, *Joyride* assumes that the robot is commanded to stop.

All the source code is available at [Ha08]. The software is approved for

REMOTE HARDWARE	ID
Desktop PC, Intel Celeron 1.7 GHz, Windows 2000	
ACER Laptop, Intel Celeron 2.6 GHz, Windows XP	TravelMate 244LC
Sanwa Supply USB-Joystick	JY-P70UR
D-Link Wireless network adapter, USB	DWL-122

Chapter 4

Adaptation

The rear joint of Marsokhod exhibits a substantial backlash. The modelling of the backlash is crucial for wheel walking with low friction.

We establish the correspondence of the duty cycle and the no load velocity. Through individual calibration of the wheels, we obtain the notion of load for each motor. We find that external torque reduces the velocity by a proportional offset.

Position, velocity, and acceleration are related by a pair of differential equations. We derive time optimal control, that we utilize for bending the joints. Tests shows that our method achieves high accuracy in practice.

4.1 Backlash compensation

While changing the inclination of the the joints, the wheels need to turn accordingly to accomplish minimal slippage. When a change in direction of the motor of the joint occurs, the joint typically does not move as long as the backlash of a few degrees is not overcome. During that period, the wheels should not perform the compensating motion either.

To measure the play in the bearings of the wheels and joints, we devise

Procedure 4.1. We strap Marsokhod to the ground, so that neither the wheels rotate nor the joints incline. Using small duty cycles of $d = \pm 0.1$, we measure the backlash in the connection bearings as

$$\bar{b} = \begin{bmatrix} 0.050 & & 0.061 & & 0.066 \\ & 0.250 & & 0.052 & \\ 0.048 & & 0.014 & & 0.041 \end{bmatrix}$$

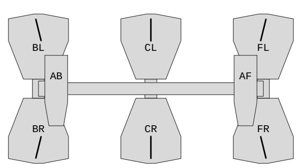

in rad. □

Since the small play in the wheel bearings is not crucial for the motion of the robot, our

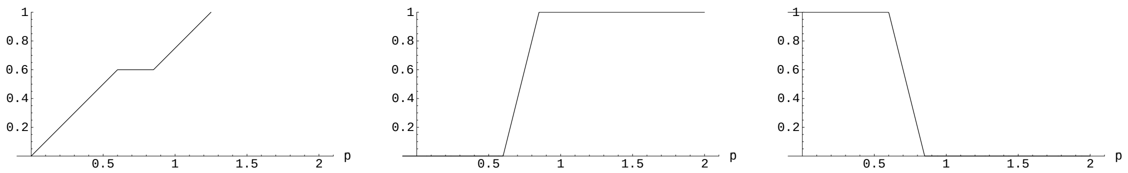

Figure 4.1: The functions $P(\bar{p},p,b)$, $P^+(\bar{p},p,b)$, and $P^-(\bar{p},p,b)$ for $p=0.6$ and $b=0.25$.

model utilizes the simplified backlash vector

$$b = \begin{bmatrix} 0 & & 0 & & 0 \\ & 0.250 & & 0.052 & \\ 0 & & 0 & & 0 \end{bmatrix}$$

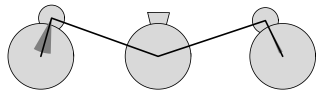

in rad. The front joint exhibits a backlash of $b_6 \approx 3$ deg. The play in the rear joint is $b_7 \approx 14$ deg.

Due to the backlash b_6, b_7, the inclination of the joint is not identical to the position of the motor shaft $\bar{p}_6$, $\bar{p}_7$. Due to the backlash, the velocity of the joint is not identical to the rate of the motor shaft $\bar{w}_6$, $\bar{w}_7$. The equations (4.1) and (4.2) model the inclination as well as the velocity of the joint.

For $b>0$, we define the functions

$P(\bar{p},p,b) :=$	$P^+(\bar{p},p,b) :=$	$P^-(\bar{p},p,b) :=$	IF
$\bar{p}$	0	1	$\bar{p} < p$
p	$(\bar{p}-p)/b$	$(b-\bar{p}+p)/b$	$p \le \bar{p} < p+b$
$\bar{p}-b$	1	0	$p+b \le \bar{p}$

In case $b=0$, we define $P(\bar{p},p,0)=\bar{p}$, $P^+(\bar{p},p,0)=1$, and $P^-(\bar{p},p,0)=1$.

We model the position and the velocity of the wheels and joints as

$$p_i^{k+1} = P(\bar{p}_i^k, p_i^k, b_i) \tag{4.1}$$

$$w_i^{k+1} = \bar{w}_i^k P^{\operatorname{sgn} \bar{w}_i^k}(\bar{p}_i^k, p_i^k, b_i) \tag{4.2}$$

for $i=0,1,\ldots,7$ with $p_i^0 = \bar{p}_i^0$.

Example 4.2. Several evaluations illustrate the principle of modelling backlash:

$$\begin{array}{lll} P(2.75,3,1)=2.75 & P^+(2.75,3,1)=0 & P^-(2.75,3,1)=1 \\ P(3.25,3,1)=3 & P^+(3.25,3,1)=0.25 & P^-(3.25,3,1)=0.75 \\ P(4.25,3,1)=3.25 & P^+(4.25,3,1)=1 & P^-(4.25,3,1)=0 \end{array}$$

□

We discuss the explicit selection of the initial values to (4.1) in the following procedure.

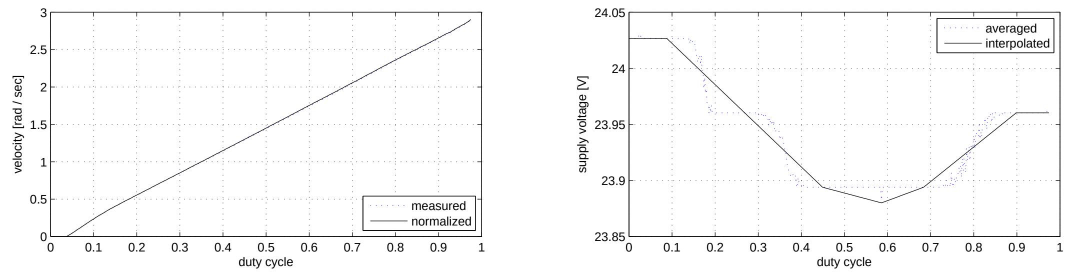

Figure 4.2: Calibration procedure recorded to obtain $V_{511}(d)$ for the motor Maxon RE 36. The voltage drop is characteristic to the power supply PS 613.

Procedure 4.3 (Initialization)**.** With joints in vertical configuration, we assign the duty cycles $d_6 = d_7 = -0.08$. In no more than 3 seconds, the motors have overcome the backlash of the joint bearings towards the negative direction before the control software is launched.

We make use of the relation $p = P(p, p, b)$. Since the joints are in vertical configuration, we set $p_6^0 := \bar{p}_6^0 = -1.2121$ rad, and $p_7^0 := \bar{p}_7^0 = 1.2121$ rad as specified in Remark 3.1 $\square$

The procedure synchronizes the configuration of the chassis with the initial variables of the software. The Figures 4.11 and 4.12 evaluate the position of the motor $\bar{p}_i^k$ and the inclination of the joint p_i^k for $i = 6, 7$ during the bending of the joint.

4.2 Calibration of the motors

The 8 motors of Marsokhod are of type Maxon RE 36 with Planetary Gearhead GP 42 C. We assume that the motors comport identically for the greater part.

At a fixed supply voltage, the no load velocity of the motor $W_{\mathsf{icr}}(d)$ depends on the duty cycle d, and the frequency defined by icr. We obtain the mapping $W_{\mathsf{icr}} : [-1, 1] \to [-\mathbf{w}, \mathbf{w}]$ in an experimental fashion:

Procedure 4.4. We adjust the reference supply voltage to $\mathbf{U} = 24$ V. We fix icr, and the direction $\mathsf{drv} = 0$ of the motor. Then, we sedately increase pwm from 0 to icr and record the velocity w measured by the encoders (3.3), and (4.2). We define

$$W_{\mathsf{icr}}(\mathsf{pwm}/\mathsf{icr}) := w\frac{\mathbf{U}}{U}$$

During operation, the supply voltage U drops, so we normalize the recorded velocity by the factor $\mathbf{U}/U$. For $d < 0$, we define $W_{\mathsf{icr}}(d) := -W_{\mathsf{icr}}(-d)$. $\square$

Let $W_{\mathsf{icr}}^{-1} : [-\mathbf{w}, \mathbf{w}] \to [-1, 1]$ be the inverse function of W_{icr}, that maps the no load velocity to the duty cycle.

When installed into the individual wheel, the velocity of the motor differs by a constant factor from the no load speed W_{icr}. We determine the scale factor for each wheel in

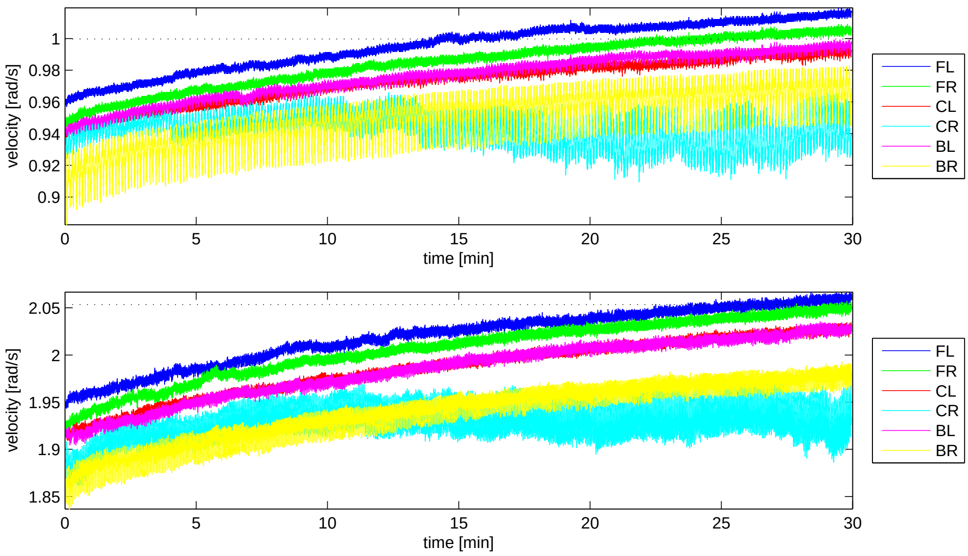

Figure 4.3: The evolvement of the wheel speeds at a constant duty cycle of $d = 35\%$ (top), and $d = 70\%$ (bottom) during the first 30 minutes after startup. The velocity is normalized by the factor $\mathbf{U}/U$.

Procedure 4.5. At $\mathbf{U} = 24$ V We accelerate the motors of the wheels up to a constant duty cycle of $d = 0.7$. Over the course of the next 30 minutes, we record the velocity, see Figure 4.3. Finally, we decelerate the motor.

The scale factor for wheel i is defined as

$$\zeta_i := \text{mean}_k \frac{\mathbf{U}}{U^k} \frac{w_i^k}{W_{\mathsf{icr}}(0.7)}$$

We obtain the following values

$$\zeta = \begin{bmatrix} 0.9713 & 0.9703 & 0.9896 \\ & \zeta_7 & & \zeta_6 & \\ 0.9469 & 0.9412 & 0.9808 \end{bmatrix}$$

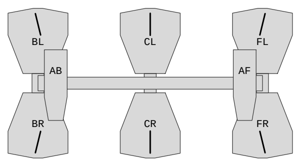

For instance, the front-left wheel rotates at $\zeta_0 = 98.96\%$ of the no load speed W_{icr} of the motor. □

The performance of the motors located inside the joints cannot be measured. Since the motor of the front joint shares a power cable with the motor in the front-right wheel, we define $\zeta_6 = \zeta_1 = 0.9808$. The motor of the rear joint shares a power cable with the motor in the back-left wheel, we define $\zeta_7 = \zeta_4 = 0.9713$.

We speculate that the rise of temperature of the motor alters the performance. Because there are no temperature sensors installed to the motors, we do not investigate the relation further.

The deviation from the no load speed of the motor is due to the friction in the bearing of the wheel. Given icr, and U, the duty cycle d correlates to the no load velocity $\hat{w}$ of a

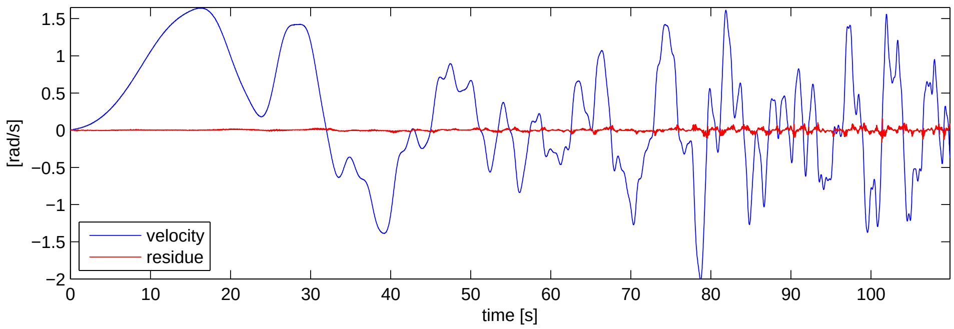

Figure 4.4: Control signal with rising frequency components to tune velocity estimation. The curve that oscillates around 0 is the difference in measured and estimated velocity.

wheel or a joint by

$$\hat{w} = \zeta W_{\mathsf{icr}}(d)\frac{U}{\bar{\mathbf{U}}} \qquad \text{and} \qquad d = W_{\mathsf{icr}}^{-1}\left(\frac{\hat{w}}{\zeta}\frac{\bar{\mathbf{U}}}{U}\right) \tag{4.3}$$

where $\bar{\mathbf{U}} = 24$ V is the nominal supply voltage as used during the calibration procedures.

Example 4.6. We compute the no load speed of the middle-right wheel $i = 3$ at the duty cycle of $d = 0.3$, with $\mathsf{icr} = 511$, and supply voltage $U = 22$ V using (4.3). Since $\zeta_3 = 0.941$ and $W_{511}(0.3) = 0.847$ rad/s, we yield $\hat{w} = 0.731$ rad/s.

At $\mathsf{icr} = 511$ and $U = 21$ V, the wheel has a no load speed of $\hat{w} = -2$ rad/s, if we assign $d = W_{511}^{-1}(\frac{-2}{\zeta_3}\frac{24}{21}) = W_{511}^{-1}(-2.429) = -W_{511}^{-1}(2.429) = 0.826$. □

Remark 4.7. A passive control that makes each wheel pick up the ambient speed is given by

$$d_i^{k+1} := W_{\mathsf{icr}}^{-1}\left(\frac{w_i^k}{\zeta_i}\frac{\bar{\mathbf{U}}}{U^k}\right)$$

for $i = 0, 1, \ldots, 5$. w_i^k is the instantaneous velocity of the wheel i measured in iteration k. □

The previous chapter documents the control of the motors $i = 0, 1 \ldots, 7$ of Marsokhod. The duty cycle d^k is updated on a discrete basis $k = 0, 1, \ldots$ at time $t = k\mathbf{h}$. Using (4.3), we define $\hat{w}^k = \zeta W_{\mathsf{icr}}(d^k)U/\bar{\mathbf{U}}$. Once, the duty cycle has changed a period of time elapses until the motor has fully responded to the control parameter. We aim to predict the no load velocity ν^k in iteration k using the linear combination

$$\nu^k = \sum_{j=0}^{\infty} \delta^j \hat{w}^{k-j} \tag{4.4}$$

To obtain the coefficients δ^j, we devise

Procedure 4.8. We fix the communication period $\mathbf{h}$, and con. Over the next 2 minutes, we assign a velocity $\hat{w}$ comprising of oscillations with increasing frequency, see Figure 4.4.

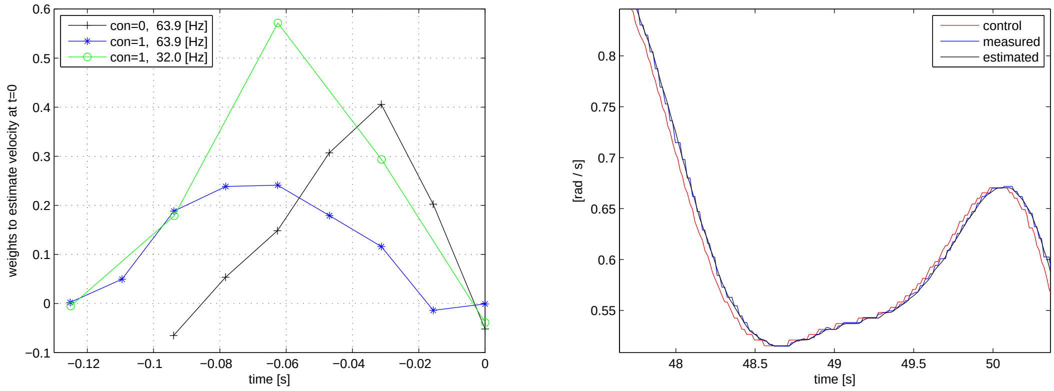

Figure 4.5: Left: Coefficients δ to estimate the velocity at time $t = 0$ s. Right: Comparison of the functions $\hat{w}^k$, w^k, and ν^k.

We solve for δ^j in $w = \sum_{j=0}^{N} \delta^j \hat{w}^{k-j}$ for a sufficiently large $N \in \mathbb{N}$ using the least square method. □

The coefficients δ^j depend on the communication period **h** and `con`. Figure 4.5 examines the coefficients. Our software uses

h [s]	`con`	δ^j for $j > 4$	δ^4	δ^3	δ^2	δ^1	δ^0
0.0157	0	0	0.1008	0.2798	0.3742	0.2452	0
0.0313	1	0	0	0.1960	0.5592	0.2449	0

Definition 4.9. We define the *load* l on the motor as the difference of measured velocity and estimated no load velocity $l = w - \nu$.

Example 4.10. Let $\mathbf{h} = 0.0157$, and `con` $= 0$. If we assign $\hat{w}^3 = 0.5$, $\hat{w}^4 = 0.6$, $\hat{w}^5 = 0.65$, and $\hat{w}^6 = 0.7$, and measure $w^7 = 0.4$. Then, $l^7 = 0.4 - 0.6332 = -0.2332$ rad/s. □

In the next section, we correlate the load l to the external torque acting on the wheel.

Field Experiment 4.11 (9. July 2008)**.** We drive Marsokhod on sandy terrain larded with obstacles of different quality. One obstruction is the tree trunk in Figure 1.1. Our objective is to observe the performance of the robot when tackling obstacles. Besides, we record the voltage supplied by the batteries to correlate the voltage drop with the driving characteristics.

During several climbing maneuvres, one or two wheels lost ground contact. Turning wheels that lack grip is futile. We present an improved load distribution in Section 6.3.

Loose connections at the `CAN` bus lines cause incidental aborts of operation. □

The voltage readings from the experiment propose an approximation of the kind

$$\mathbf{U} - U = \xi \sum_{i=0}^{7} |d_i| + \Xi \sum_{i=0}^{7} l_i^2 \tag{4.5}$$

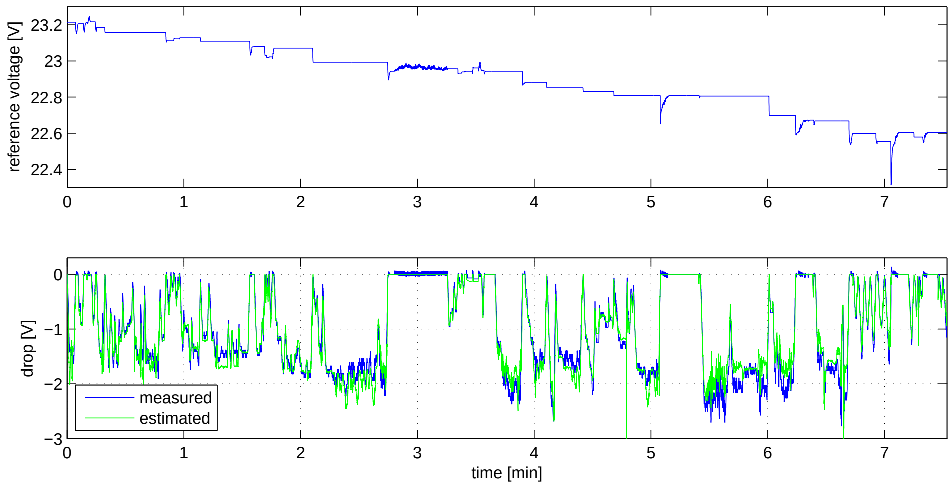

Figure 4.6: Recording of voltages $\mathbf{U}$ (top), and $U - \mathbf{U}$ (bottom) during the Field Experiment 4.11. The voltage drop is correlated with the total duty cycles and loads on the wheels.

Specific to the pairs of batteries 2×HYS1240, as well as 2×HYS1250 that mobilize Marsokhod, we yield the factors $\xi = 0.6$ V and $\Xi = 0.4$ Vs^2/rad^2. Figure 4.6 demonstrates the quality of the approximation.

While driving Marsokhod in the field, we utilize (4.5) to prevent a voltage drop below a certain threshold, see Section 6.1.

Remark 4.12. We inspect relation (4.5) with respect to the 6 wheels, thus neglecting the joints. The power usage is optimal when $\sum_{i=0}^{5} l_i^2 = 0$. Remark 4.7 explains how to maintain this state. The control reduces the sum of absolute load: The wheels do not resist external torques, and the motors pick up the ambient speed.

When driving up a slope, load on the wheels $\sum_{i=0}^{5} l_i^2 > 0$ is unavoidable. We assume the overall control $\sum_{i=0}^{5} |d_i|$ is constant. Then, the power usage (4.5) is optimal when $\mathrm{var}(l) = \frac{1}{6} \sum_{i=0}^{5} (l_i - \bar{l})^2$ is minimal. The implication is to increase the speed of wheels with low load and decrease the speed of wheels with high load. Section 6.3 explains why this choice usually deteriorates the performance. □

4.3 Quantification of load

An external torque τ on a wheel causes a difference in the measured velocity w and the no load velocity ν defined in (4.4). Our experiments show that the velocity defect l is proportional to the torque τ on the motor. Moreover, the relation depends on the duty cycle d of the motor, the modulation frequency icr, and the sign of the product τd. We model the relation as

$$l = w - \nu = \tau B_{\mathsf{icr}}^{\operatorname{sgn} \tau d}(d) \tag{4.6}$$

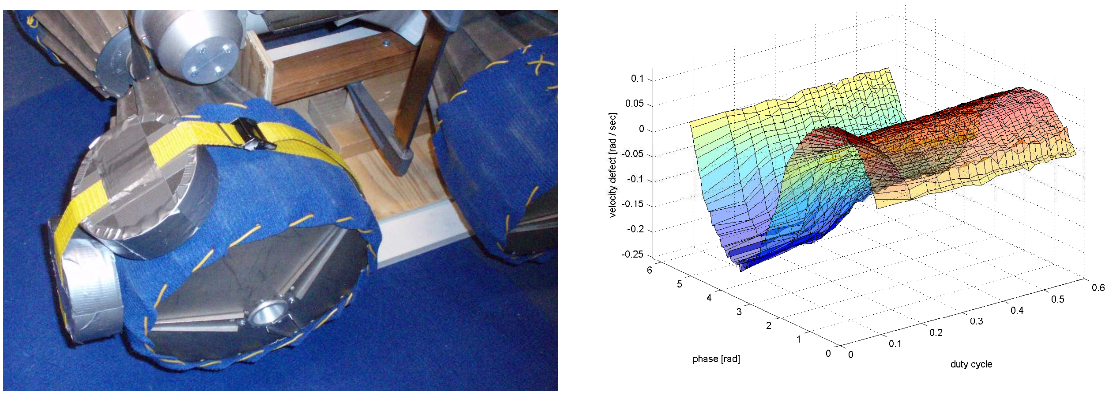

Figure 4.7: Left: The weights excert a peak torque of 5.51 Nm. Right: The recording of $(w - \nu)(\alpha, d)$ where $\mathsf{icr} = 511$.

$B^+_{\mathsf{icr}}, B^-_{\mathsf{icr}} : [-1, 1] \to \mathbb{R}$ map the duty cycle to numbers with unit rad/(sNm). The functions are determined through

Procedure 4.13. We strap a metallic weight tightly to the front-left wheel of Marsokhod. Figure 4.7 shows the setup. We sedately increase the duty cycle in the range $d \in [0, 0.6]$.

We record the difference l of the measured velocity w and the no load velocity ν with respect to the angular phase $\alpha \in [0, 2\pi)$ and the duty cycle d. Since the weight is installed at a fixed spot, the external torque on the wheel is periodic after one revolution. During one revolution, the torque $\tau(\alpha)$ oscillates with amplitude 5.51 Nm. We extract the functions $B^{\pm}_{\mathsf{icr}}$ from the equations

$$(w - \nu)(\alpha, d) = \tau(\alpha) \cdot \begin{cases} B^+_{\mathsf{icr}}(d) & \text{if } 0 \le \alpha < \pi \\ B^-_{\mathsf{icr}}(d) & \text{if } \pi \le \alpha < 2\pi \end{cases}$$

Figure 4.7 illustrates $(w - \nu)(\alpha, d)$ for $\mathsf{icr} = 511$. Naturally, $\tau(\alpha)$ resembles $\sin(\alpha)$. □

We execute the procedure for $\mathsf{icr} = 255, 511, 1023$, and 2047. The functions $B^{\pm}_{\mathsf{icr}}$ are depicted in Figure 4.8: A reduced modulation frequency increases the load resistance at small duty cycles. At a low modulation frequency, the results justify the simplification

$$l = w - \nu \simeq \tau \cdot \begin{cases} 0.030 & \text{if } 0 \le \tau d \\ 0.015 & \text{if } \tau d < 0 \end{cases} \tag{4.7}$$

which is an important observation for any linear control algorithm.

The next procedure confirms that the rhs of (4.6) does not depend on the supply voltage.

Procedure 4.14. A different weight strapped to the wheel now excerts a peak torque of ± 2.98 Nm. We set $\mathsf{icr} = 1023$ and repeat Procedure 4.13 four times with supply voltages $\mathbf{U} = 24, 22, 20$, and 16 V, respectively. □

Figure 4.8 exhibits the results. Apparently, the defect in velocity is not susceptible to the supply voltage $16 \le \mathbf{U} \le 24$ V.

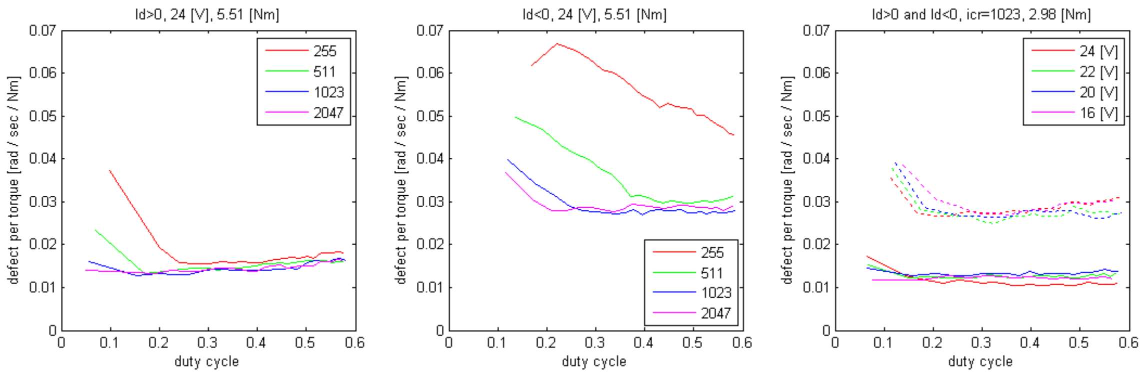

Figure 4.8: The functions B^{+}_{icr} (left), and B^{-}_{icr} (middle) for different modulation frequencies of $31.25, 15.63, 7.81$, and 3.91 kHz. Right: The functions $B^{\pm}_{1023}$ obtained from the experiment at different supply voltages.

4.4 Position and velocity control

In order to vary the inclination of the joints of Marsokhod, we implement position control with bounded velocity. We utilize the same model to accelerate the forward drive and the turning. The theory is presented in

Lemma 4.15. With a coefficient $\mu > 0$ and for a constant c, we investigate the differential equations

$$\partial_t p(t) = v(t) \tag{4.8}$$

$$\partial_t v(t) = \mu(c - v(t)) \tag{4.9}$$

Using Laplace[1]-transformation and integration, we obtain the solution as

$$p(t) = p_0 + v_0 \frac{1}{\mu}(1 - e^{-t\mu}) - c\frac{1}{\mu}(1 - t\mu - e^{-t\mu}) \tag{4.10}$$

$$v(t) = v_0 e^{-t\mu} + c(1 - e^{-t\mu}) \tag{4.11}$$

where (v_0, p_0) represents the instantaneous state $(v(0), p(0))$. We bound the parameter $|c| \leq C$, and assume $|v_0| \leq C$. According to (4.9), these bounds limit $|v| \leq C$, and $|v'| \leq 2\mu C$.

We are interested in the choice of parameter c with $|c| \leq C$ to reach a target state $(v_\mathrm{d}, p_\mathrm{d})$ from the instantaneous state (v_0, p_0) in least time. The time T to attain $v(T) = v_\mathrm{d}$ with $c = C\,\mathrm{sgn}\,(v_\mathrm{d} - v_0)$ is $T = \frac{1}{\mu}\log\frac{c - v_0}{c - v_\mathrm{d}}$. We evaluate

$$p(T) = p_0 + \frac{1}{\mu}\left(v_0 - v_\mathrm{d} + c\log\frac{c - v_0}{c - v_\mathrm{d}}\right)$$

which does not necessarily equal p_d. For convenience, we define $p_T = p(T)$. Time-optimal control is achieved with $c = C\,\mathrm{sgn}\,(p_\mathrm{d} - p_T)$. □

[1] Pierre Simon Laplace, * 23. Mar 1749 in Beaumont-en-Auge, † 5. Mar 1827 in Paris

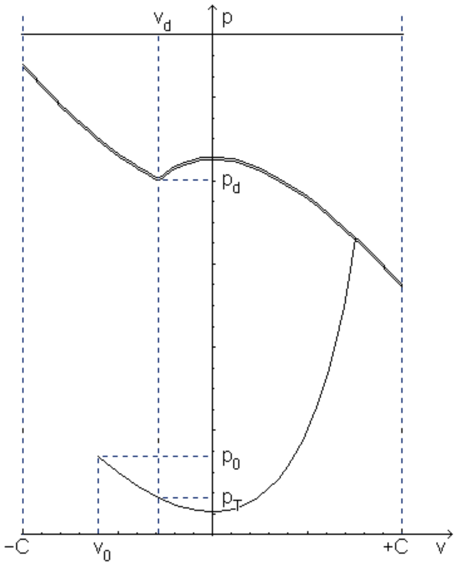

Figure 4.9: Phase plot to Lemma 4.15. The sign of the control $c = \pm C$ at time $t = 0$ depends on whether (v_0, p_0) lies above or underneath the bold line that contains $(v_\mathrm{d}, p_\mathrm{d})$.

To apply the theory in the lemma, we discretize the functions (4.10) and (4.11) as

$$p^{k+1} = p^k + v^k \frac{1}{\mu}(1 - e^{-\mathbf{h}\mu}) - c^k \frac{1}{\mu}(1 - \mathbf{h}\mu - e^{-\mathbf{h}\mu}) \tag{4.12}$$

$$v^{k+1} = v^k e^{-\mathbf{h}\mu} + c^k(1 - e^{-\mathbf{h}\mu}) \tag{4.13}$$

where $\mathbf{h}$ is the period of one communication cycle. The parameter $c^k \in [-C, C]$ is selected based on the type of control:

Velocity control: To reach and maintain the destination velocity v_d, we set

$$c^k = \mathcal{C}(v_\mathrm{d}) := \mathrm{clip}\big(-C, \frac{v_\mathrm{d} - (1 - \mathbf{h}\mu)v^k}{\mathbf{h}\mu}, C\big) \tag{4.14}$$

where $\mathrm{clip}\,(a, b, c) := \min(\max(a, b), c)$.

Position and velocity control: To attain the state $(v_\mathrm{d}, p_\mathrm{d})$, we set

$$c^k = \mathcal{C}(v_\mathrm{d}, p_\mathrm{d}) := C\,\mathrm{sgn}\big(p_\mathrm{d} - p^k - \frac{1}{\mu}(v^k - v_\mathrm{d} + c\log\frac{c - v^k}{c - v_\mathrm{d}})\big) \tag{4.15}$$

where $c = C\,\mathrm{sgn}\,(v_\mathrm{d} - v^k)$.

Velocity control with bounded position: To reach and maintain the destination velocity v_d with the constraint $p_{\min} \le p \le p_{\max}$, we set

$$c^k = \mathcal{C}(v_\mathrm{d}, p_{\min}, p_{\max}) := \mathrm{clip}\big(\mathcal{C}(0, p_{\min}), \mathcal{C}(v_\mathrm{d}), \mathcal{C}(0, p_{\max})\big) \tag{4.16}$$

Because of $\mathcal{C}(v_\mathrm{d}) = \mathcal{C}(v_\mathrm{d}, -\infty, \infty)$, equation (4.14) is contained in (4.16). In case $v_\mathrm{d} = 0$, the control (4.15) is a special case of (4.16), since $\mathcal{C}(0, p_\mathrm{d}) = \mathcal{C}(0, p_\mathrm{d}, p_\mathrm{d})$.

Example 4.16. Figure 4.10 demonstrates the three types of control. □

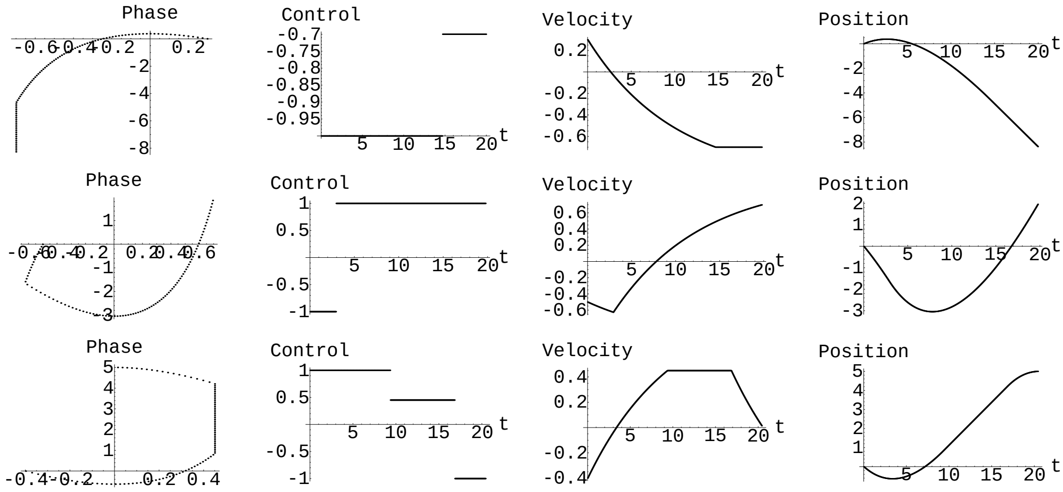

Figure 4.10: Illustration of the three types of control with $\mu = 0.1$, $C = 1$, and $p_0 = 0$. Top: Velocity control with $v_0 = 0.3$, and $v_\mathrm{d} = -0.7$. Middle: Position and velocity control $v_0 = -0.5$, and $(v_\mathrm{d}, p_\mathrm{d}) = (0.7, 2)$. Bottom: Velocity control with bounded position $v_0 = -0.4$, $v_\mathrm{d} = 0.45$, while $p_{\min} = -5$, and $p_{\max} = 5$.

To control the inclination of the front joint of Marsokhod, the motor is assigned a velocity $\hat{w}_6(t)$ of the form (4.11). According to the equation, the function $\hat{w}_6(t)$ is continous. Using the conversion (4.3), the velocity $\hat{w}_6(t)$ translates into a continous duty cycle

$$d_6(t) := W_{\mathsf{icr}}^{-1}\left(\frac{\hat{w}_6(t)}{\zeta_6}\frac{\mathbf{U}}{U}\right)$$

Since the slope of the duty cycle $d_6(t)$ is limited, we guarantee low mechanical stress on the motor as well as on the chassis of Marsokhod. We test the accuracy of the position control in

Procedure 4.17. Marsokhod is located on flat terrain. We assign a sequence of target positions p_6^d to be attained by the front joint

$$p_6^\mathrm{d} = -2.21 \;\rightarrow\; -2.51 \;\rightarrow\; -1.61 \;\rightarrow\; -1.81 \;\rightarrow\; -1.21$$

while $v_6^\mathrm{d} = 0$. The transition to the next element in the sequence occurs when $|p_6 - p_6^\mathrm{d}| \leq 0.05$ [rad] during a period of 1 s. Then, the joint has attained the target position up to a certain accuracy and has stopped moving. At the beginning, the joint is in vertical position $p_6 = -1.2121$ rad, recalling that $\gamma_f = -p_6$. The initial position of the motor is $\bar{p}_6 = -1.2121 + b_6$. Figure 4.11 evaluates the positions $\bar{p}_6, p_6$ and the velocities $\hat{w}_6, w_6$.

Analogous, we assign a sequence of target positions p_7^d to be attained by the rear joint

$$p_7^\mathrm{d} = 2.21 \;\rightarrow\; 2.51 \;\rightarrow\; 1.61 \;\rightarrow\; 1.81 \;\rightarrow\; 1.21$$

At the beginning, the joint is in vertical position $p_7 = 1.2121$ rad, recalling that $\gamma_r = p_7$. The initial position of the motor is $\bar{p}_7 = 1.2121$ rad. Figure 4.12 evaluates the positions $\bar{p}_7, p_7$ and the velocities $\hat{w}_7, w_7$. $\square$

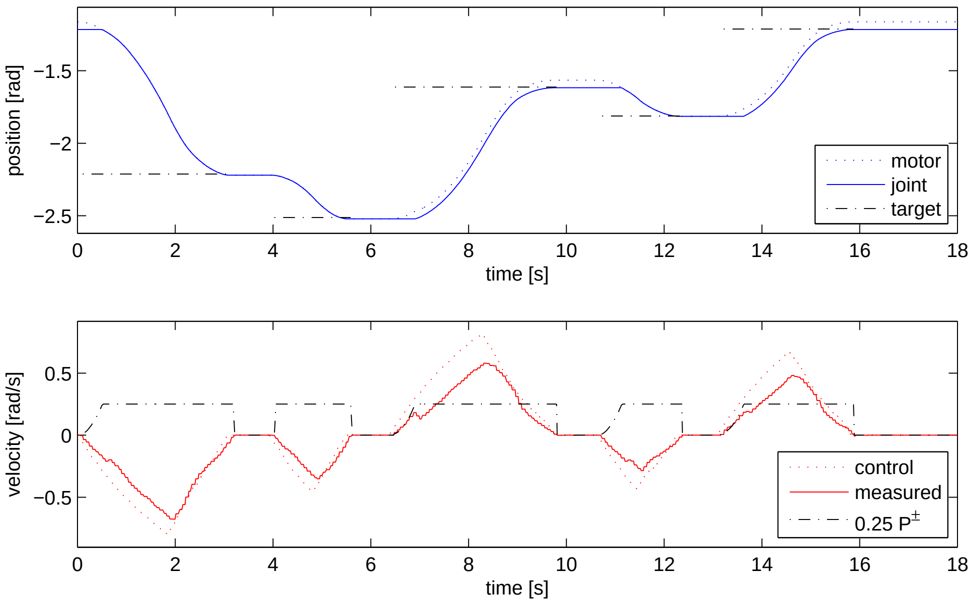

Figure 4.11: Position control of the front joint of Marsokhod using (4.15) with the parameters $\mu = 0.4$, $C = \frac{1}{2}\mathbf{w}$. The position of the motor $\bar{p}_6$ and the inclination of the joint p_6 deviate at most by the backlash of $b_6 = 0.052$ [rad]. The lower frame evaluates $P^{\operatorname{sgn} w_6}(\bar{p}_6, p_6, b_6)$, which is not a velocity but a scalar.

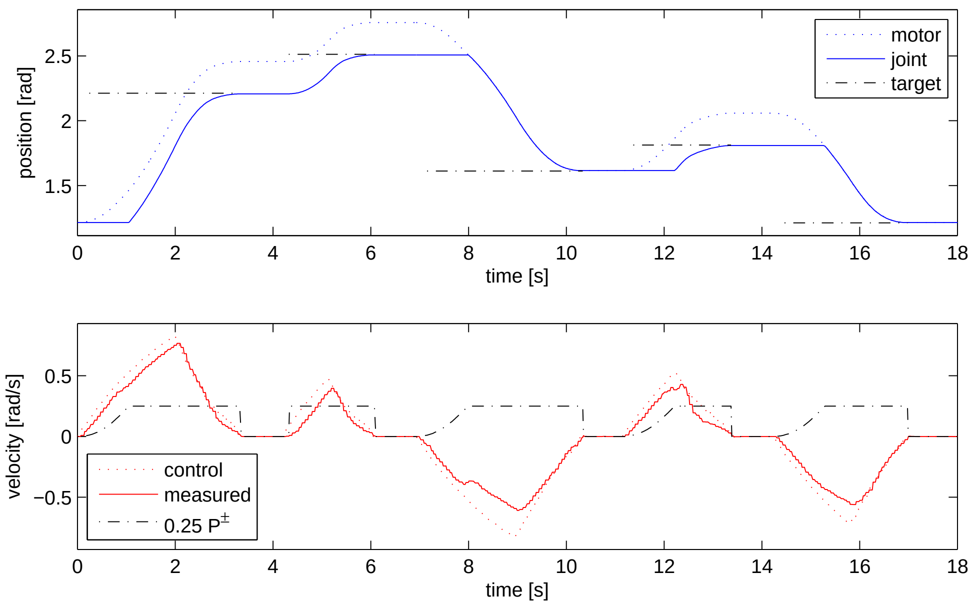

Figure 4.12: Position control of the rear joint of Marsokhod. The position of the motor $\bar{p}_7$ and the inclination of the joint p_7 deviate at most by the backlash of $b_7 = 0.250$ rad. The lower frame evaluates the scalar $P^{\operatorname{sgn} w_7}(\bar{p}_7, p_7, b_7)$.

Chapter 5

Mobility

The elementary motions of Marsokhod are

STYLE	MATRIX	CONTROL	PARAMETERS
drive straight	m_1	(4.14)	v_1^{d}
spin around the center of the center axle	m_2	(4.14)	v_2^{d}
drift sidewards, complements m_1 and m_2	m_3	(4.14)	v_3^{d}
trench with front-right wheel	m_4	(4.14)	v_4^{d}
bend the front joint	m_6	(4.16)	$v_6^{\mathrm{d}}, p_6^{\min}, p_6^{\max}$
bend the rear joint	m_7	(4.16)	$v_7^{\mathrm{d}}, p_7^{\min}, p_7^{\max}$

We represent these motions as matrices m_j for $j \in J := \{1, 2, 3, 4, 6, 7\}$ that depend on the instantaneous state of the robot. The matrix m_5 is reserved for future use.

The 6-wheeled Marsokhod drives forward and backward, if we assign the speeds $\hat{w} = m_1 v_1$ for a suitable factor $v_1 \in \mathbb{R}$ where

$$m_1 = \begin{bmatrix} 1 & & 1 & & 1 \\ & 0 & & 0 & \\ 1 & & 1 & & 1 \end{bmatrix}$$

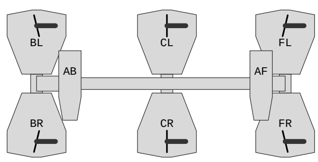

For instance, to drive the robot ahead with velocity 0.27 m/s, we set $v_1 = 0.27/\mathbf{r} = 2.25$ rad/s. The matrices m_2, m_3, m_4, m_6, m_7 are introduced in the next sections. We utilize the quantities sketched in Figure 3.3:

	VAR	
bending of front joint	γ_f	$= -p_6$
clearance of front to center axle	c_f	$= \sqrt{\mathbf{a}^2 + \mathbf{b}^2 - 2\mathbf{ab} \cos \gamma_f}$
inclination of front lever	α_f	$= \arccos\big((\mathbf{b}^2 + c_f^2 - \mathbf{a}^2)/2\mathbf{b}c_f\big)$
bending of rear joint	γ_r	$= +p_7$
clearance of rear to center axle	c_r	$= \sqrt{\mathbf{a}^2 + \mathbf{b}^2 - 2\mathbf{ab} \cos \gamma_r}$
inclination of rear lever	α_r	$= \arccos\big((\mathbf{b}^2 + c_r^2 - \mathbf{a}^2)/2\mathbf{b}c_r\big)$

Figure 5.1: Left: Contact with low friction when skidding. Right: High friction.

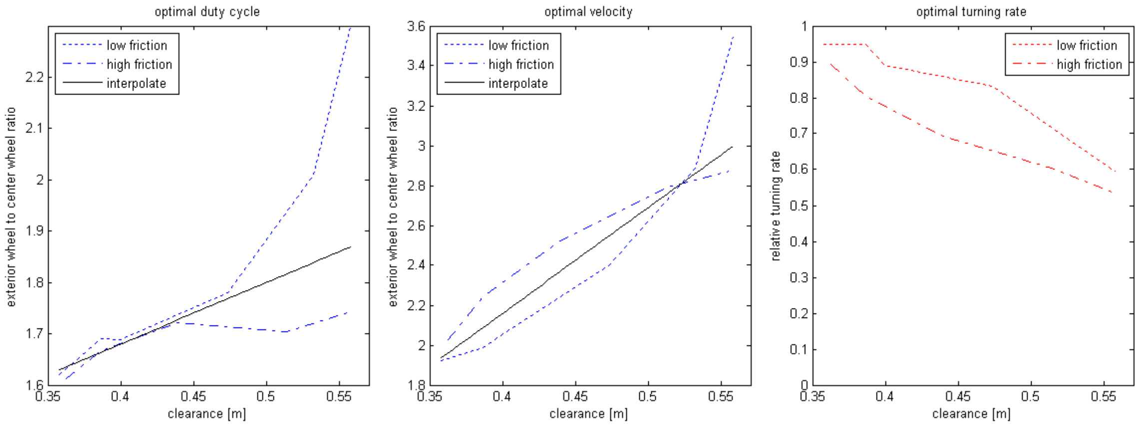

Figure 5.2: Left: Efficient duty cycle ratios for turning. Center: Numerical data $\hat{F}(c)$ to obtain $F(c)$. Right: Generally, an increased axle distance lowers the turning rate.

5.1 Spin

Marsokhod spins around the center of the center axle, if we assign a multiple of m_2 as wheel speeds, where

$$m_2 = \begin{bmatrix} -F(c_r) & & -1 & & -F(c_f) \\ & 0 & & 0 & \\ F(c_r) & & 1 & & F(c_f) \end{bmatrix}$$

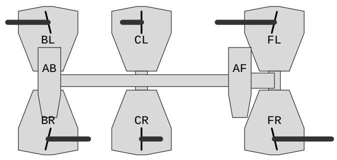

The velocities of the wheels of the exterior axles depend on the offsets c_f, and c_r. In the illustration next to the matrix, we have $c_f = 0.558$ m, and $c_r = 0.392$ m. The definition of the function as $F(c) := 5.3c + 0.04$ is the result of

Procedure 5.1. Marsokhod is at rest on a flat surface of homogeneous texture. The joints are adjusted so that the axles are equidistant $c = c_f = c_r$. We assign the duty cycle

$$d(\tau) = 0.8 \begin{bmatrix} +\frac{1}{2}(1+\tau) & & +(1-\tau) & & +\frac{1}{2}(1+\tau) \\ & 0 & & 0 & \\ -\frac{1}{2}(1+\tau) & & -(1-\tau) & & -\frac{1}{2}(1+\tau) \end{bmatrix}$$

where τ ranges slowly from 0 to 1. The sum $\sum_i |d_i(\tau)|$ is constant for all $\tau \in [0, 1]$, which corresponds to an invariant level of energy. We define

$$\hat{F}(c) := \frac{\frac{1}{4}(w_0 - w_1 + w_4 - w_5)}{\frac{1}{2}(w_2 - w_3)}$$

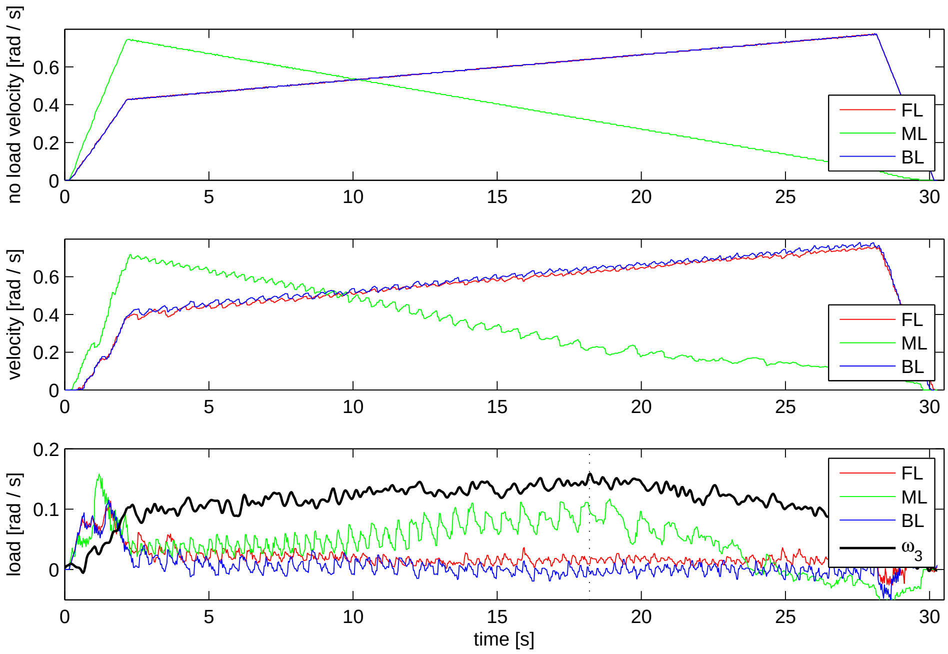

Figure 5.3: Illustration to Procedure 5.1. The axles are equidistant $c_f = c_r = 0.532$ m. The dashed line indicates, that the maximum turning rate occurs at $t = 18.2$ s. According to the measured velocities, we define $\hat{F}(c_f) = 2.8$ rad/s.

where w_i are the velocities of the wheels in the instant when the maximum turning rate ω_3 is achieved. $\square$

The procedure is carried out for various axle distances c, and on two different ground materials, see Figure 5.1. The ratio $\hat{F}$ for optimal turning is plotted in Figure 5.4. The function F is a linear approximation to $\hat{F}$.

We state the criteria to turn Marsokhod efficiently: The wheels of the center axle should not slip, but bear as much load as possible. The wheels of the exterior axles are required to move faster by a factor $F(c_f)$, and $F(c_r)$ respectively. A reduced wheel base means faster turning – ideally c_f, c_r are as small as possible.

5.2 Sidewards drift and trenching

The matrix

$$m_3 = \begin{bmatrix} 1 & 0 & -1 \\ 0 & 0 & \\ -1 & 0 & 1 \end{bmatrix}$$

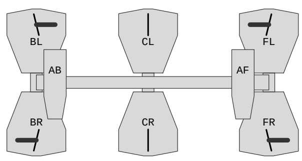

complements m_1 and m_2. On granular soil, we expect the robot to drift sidewards, if we assign $m_3 v_3$ to the wheels for $v_3 \in (-\mathbf{w}, \mathbf{w})$. Due to the configuration of the spikes, we

Figure 5.4: Photographs from the Field Experiment 5.2. Marsokhod on sandy as well as on rocky terrain.

assume that the grains exit the wheel slightly sideways. However, the effect is negligible in practice:

Field Experiment 5.2 (4. Jul 2008)**.** Marsokhod was operated on the artificial pile of sand and stones that serves as a test bed for the field robots of the laboratory. The rover was powered by batteries and controlled by the operator with a laptop computer using wireless communications.

The test showed that the utilization of m_3 does not propel Marsokhod sideways. Instead, the wheels of the exterior axles trenched the sand.

On rocky ground, a number of stones got stuck between the blades of the wheels. Due to the nearly uninterrupted driving, and the condition of the batteries, the power depleted after 40 min. The wireless communication broke down a few times. □

Quote 2.2 states that Marsokhod has the capability of ripping-up the surface ground layer. The motion that employs the front-right wheel to dig is

$$m_4 = \begin{bmatrix} 0 & & 0 & & 0 \\ & 0 & & 0 & \\ 0 & & 0 & & 1 \end{bmatrix}$$

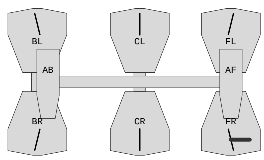

From a standing position, Marsokhod excavates a layer of up to 9 cm of sand as demonstrated by Field Experiment 6.3.

5.3 Wheel walking

Using elementary geometry, we derive proper wheel velocities to accompany the bending of the joints. The objective is to avoid slippage. Then, we present the common modes of wheel walking.

A mechanism inside the joint prevents external load on the joint motor. The lock is suspended when the motor inside the joint spins and the backlash is overcome. We define

$$m_6 = \begin{bmatrix} 0 & & 0 & & 0 \\ & 0 & & 1 & \\ 0 & & 0 & & 0 \end{bmatrix}$$

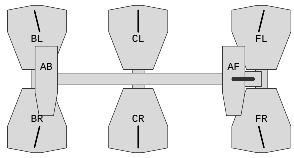

and

$$m_7 = \begin{bmatrix} 0 & & 0 & & 0 \\ & 1 & & 0 & \\ 0 & & 0 & & 0 \end{bmatrix}$$

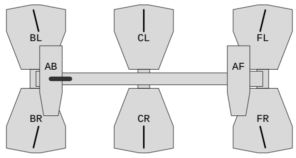

To rotate the front joint, we assign the velocities $m_6 v_6$ with $v_6 \in (-\mathbf{w}, \mathbf{w})$. To rotate the rear joint, we assign the velocities proportional to m_7.

The motion of the joints is escorted by a rotation of the wheels. Turning the wheels at the appropriate rate compensates the change in axle distance as well as in the inclination of the bearings. We derive these rates in

Lemma 5.3. The following relations are true for any triangle in the plane such as

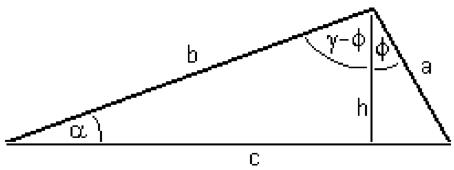

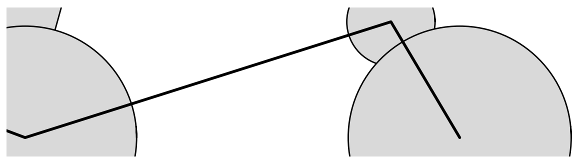

From the law of cosine

$$c = \sqrt{a^2 + b^2 - 2ab\cos\gamma(t)} \qquad \text{we obtain} \qquad \partial_t c = \gamma'(t)\frac{ab\sin\gamma(t)}{c}.$$

Let the perpendicular h to side c split $\gamma(t)$ into the angles $\gamma(t) - \phi$ and ϕ. Using the relations $\cos\phi = \frac{h}{a}$, and $\cos(\gamma(t) - \phi) = \frac{h}{b}$, we distill

$$\phi = \arccos\frac{b\sin\gamma(t)}{c} \qquad \text{with derivative} \qquad \partial_t\phi = \gamma'(t)\frac{b(b - a\cos\gamma(t))}{c^2}$$

and

$$h = \frac{ab\sin\gamma(t)}{c} \qquad \text{with} \qquad \partial_t h = \gamma'(t)ab\left(\frac{\cos\gamma(t)}{c} - \frac{ab\sin^2\gamma(t)}{c^3}\right).$$

Additionally, we have

$$\partial_t\big(\gamma(t) - \phi\big) = \gamma'(t)\frac{a(a - b\cos\gamma(t))}{c^2}.$$

□

The graphics in Lemma 5.3 motivate the transcription of the formulas to the coordinate system of Marsokhod: The change in inclination of the front joint is w_6 as argued in (4.2).

For smooth wheel walking, we contribute $m_6 v_6 + n_6 w_6$ to the motor velocities $\hat{w}$, where the matrix

$$n_6 = \begin{bmatrix} (1-\rho_f)u & (1-\rho_f)u + \frac{1}{2}\frac{\mathbf{a}(\mathbf{a}-\mathbf{b}\cos\gamma_f)}{c_f^2} & -\rho_f u - \frac{\mathbf{b}(\mathbf{b}-\mathbf{a}\cos\gamma_f)}{c_f^2} \\ 0 & & 0 \\ (1-\rho_f)u & (1-\rho_f)u + \frac{1}{2}\frac{\mathbf{a}(\mathbf{a}-\mathbf{b}\cos\gamma_f)}{c_f^2} & -\rho_f u - \frac{\mathbf{b}(\mathbf{b}-\mathbf{a}\cos\gamma_f)}{c_f^2} \end{bmatrix} \tag{5.1}$$

with $u = \frac{\mathbf{ab}\sin\gamma_f}{\mathbf{r}c_f}$ and $\rho_f \in [0,1]$.

The change in inclination of the rear joint is w_7. While the joint bends, we contribute $m_7 v_7 + n_7 w_7$ to the motor velocities $\hat{w}$, where the matrix

$$n_7 = \begin{bmatrix} -\rho_r u - \frac{\mathbf{b}(\mathbf{b}-\mathbf{a}\cos\gamma_r)}{c_r^2} & (1-\rho_r)u + \frac{1}{2}\frac{\mathbf{a}(\mathbf{a}-\mathbf{b}\cos\gamma_r)}{c_r^2} & (1-\rho_r)u \\ 0 & & 0 \\ -\rho_r u - \frac{\mathbf{b}(\mathbf{b}-\mathbf{a}\cos\gamma_r)}{c_r^2} & (1-\rho_r)u + \frac{1}{2}\frac{\mathbf{a}(\mathbf{a}-\mathbf{b}\cos\gamma_r)}{c_r^2} & (1-\rho_r)u \end{bmatrix} \tag{5.2}$$

with $u = \frac{\mathbf{ab}\sin\gamma_r}{\mathbf{r}c_r}$ and $\rho_r \in [0,1]$.

Example 5.4. Let $\mathbf{r} = 0.125$ m, $\gamma_f = 2.1$, and $\rho_f = 0.4$. Then,

$$m_6 + n_6 = \begin{bmatrix} 0.4942 & 0.5331 & -1.1261 \\ 0 & & 1 \\ 0.4942 & 0.5331 & -1.1261 \end{bmatrix}$$

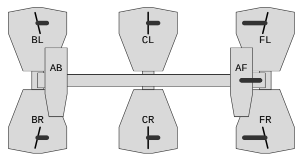

With $\mathbf{r} = 0.115$ m, $\gamma_r = 1.85$, and $\rho_r = 0$ we yield

$$m_7 + n_7 = \begin{bmatrix} -0.8329 & 1.0801 & 1.0562 \\ 1 & & 0 \\ -0.8329 & 1.0801 & 1.0562 \end{bmatrix}$$

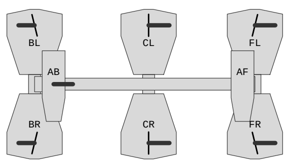

□

The matrices n_6, n_7 compensate the joint motion, so that on a flat surface neither wheel rips up the soil. For $\rho = 0$, the exterior axle of the joint is static while the joint bends. For $\rho = 1$, the other two axles remain static.

The position of the joints p_6, and p_7 are restrained to $p_6^{\min} \leq p_6 \leq p_6^{\max}$, and $p_7^{\min} \leq p_7 \leq p_7^{\max}$. Attempts to move the joint beyond these intervals might damage the hardware of the robot.

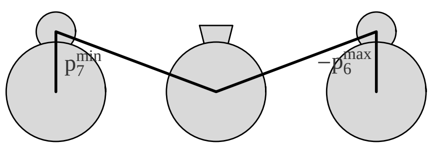

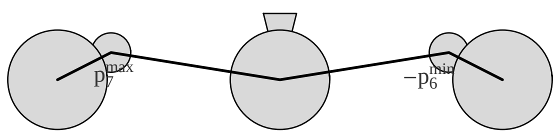

In our model, we choose

$$\begin{aligned} p_6^{\min} &= -2.55 & \qquad p_7^{\min} &= \arccos \mathbf{a}/\mathbf{b} \\ p_6^{\max} &= -\arccos \mathbf{a}/\mathbf{b} & \qquad p_7^{\max} &= 2.55 \end{aligned} \tag{5.3}$$

For increased safety, these bounds do not exhaust the physical limits.

In the configuration $\gamma = \arccos \mathbf{a}/\mathbf{b}$ and $\rho = 1$, the motors in the wheels need to turn faster than the motor of the joint by a factor of up to 2.261. Therefore, the joint velocities w_6, w_7 are controlled with care.

With the aid of the position control described in Section 4.4, conventional wheel walking *rolking* is performed as

p_7^{d}	ρ_r	STATE $p(0)$	p_6^{d}	ρ_f
$p_7^{\min}$		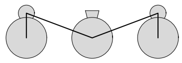	$p_6^{\min}$	1
$p_7^{\max}$	1	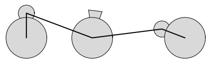	$p_6^{\max}$	0
$p_7^{\min}$	1	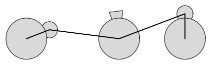	$p_6^{\max}$	
$\downarrow$	$\downarrow$	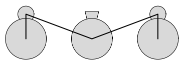	$\downarrow$	$\downarrow$

Values of ρ_f, ρ_r are omitted when irrelevant. The transition to the next state occurs, when both joints have obtained the target inclination p_6^{d}, p_7^{d} and the motors are stopped $v_6^{\mathrm{d}} = 0$, $v_7^{\mathrm{d}} = 0$. The schemes of front-wheel walking and worm-like advancement are

STATE $p(0)$	p_6^{d}	ρ_f
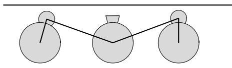	$p_6^{\min}$	1
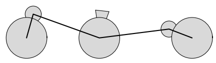	$p_6^{\max}$	0
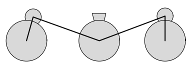	$\downarrow$	$\downarrow$

p_7^{d}	ρ_r	STATE $p(0)$	p_6^{d}	ρ_f
$p_7^{\max}$	0	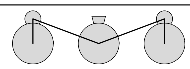	$p_6^{\min}$	1
$p_7^{\min}$	1	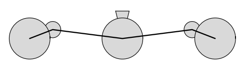	$p_6^{\max}$	0
$\downarrow$	$\downarrow$	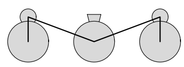	$\downarrow$	$\downarrow$

Rear-wheel walking and rolking with extended wheel base is carried out as

p_7^{d}	ρ_r	STATE $p(0)$
$p_7^{\max}$	0	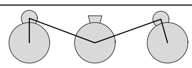
$p_7^{\min}$	1	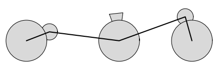
$\downarrow$	$\downarrow$	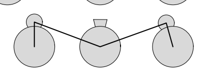

p_7^{d}	ρ_r	STATE $p(0)$	p_6^{d}	ρ_f
$p_7^{\max}$	1	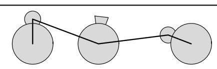	$p_6^{\max}$	0
$p_7^{\min}$	1	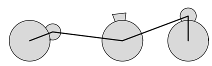	$p_6^{\min}$	1
$\downarrow$	$\downarrow$	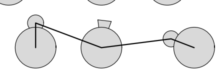	$\downarrow$	$\downarrow$

Several transitions intend to keep the exterior axles at their place. In practice, the front and rear joints might not move with perfect synchronization. The backlash in the rear joints is greater than in the front joint, and takes more time to overcome. The load on the joints might differ. The velocities of the exterior axles a_f, a_r are

$$\begin{aligned} a_f &= -\rho_f y_f + (1-\rho_r) y_r \\ a_r &= -\rho_r y_r + (1-\rho_f) y_f \end{aligned} \qquad \text{where} \qquad \begin{aligned} y_f &= \tfrac{\mathbf{ab}\sin\gamma_f}{\mathbf{r}c_f} v_6 \\ y_r &= \tfrac{\mathbf{ab}\sin\gamma_r}{\mathbf{r}c_r} v_7 \end{aligned}$$

The squared deviation from zero $a_f^2 + a_r^2$ is minimal for

$$\rho_f = \frac{y_f^2 + (2\epsilon - 1)y_f y_r + 2\epsilon y_r^2}{2(y_f^2 + y_r^2)} \qquad \text{and} \qquad \rho_r = \frac{2(1-\epsilon)y_f^2 + (1-2\epsilon)y_f y_r + y_r^2}{2(y_f^2 + y_r^2)}$$

where ϵ equals the desired value of ρ_f. For instance, in the transition CNT *0* $\rightarrow$ *1* above, we choose $\epsilon = 0$.

Remark 5.5. The different wheel walking modes are commanded in both, forward and reverse direction using only 4 buttons of a joystick. We define the sequence

$$\varrho^{k+1} = \begin{cases} 0 & \text{if } v_1^{\mathrm{d}} > 0 \quad \text{intention to drive forward} \\ 1 & \text{if } v_1^{\mathrm{d}} < 0 \quad \text{intention to drive backward} \\ \varrho^k & \text{if } v_1^{\mathrm{d}} = 0 \quad \text{most recent intention} \end{cases}$$

with $\varrho^0 = 0$, where v_1^{d} represents the instantaneous target velocity that scales the forward motion. The value ϱ estimates the principle driving direction: $\varrho = 0$ for forward, $\varrho = 1$ backward. The factors ρ_f, ρ_r are selected on the basis of ϱ as

INTENTION	ρ_f	ρ_r
increase c_f, c_r	$1-\varrho$	ϱ
decrease c_f, c_r	ϱ	$1-\varrho$

For instance, if the operator intends to increase c_r after backing up the robot, i.e. $v_1^{\mathrm{d}} < 0$ and $\varrho = 1$, then $\rho_r = 1$. The rear axle reverses in the backward direction. □

Field Experiment 5.6 (14. July 2008)**.** Due to a drizzle, we covered the electronics with a polythene sheet. Marsokhod was launched from the lander platform, see Figure 2.3, that we positioned in the unmown meadow opposite to the machine shop. The rolking modes were tested successfully. The robot was operator-controlled using a joystick.

Turning the robot on grass was stressful; the blades of the wheels were retained by the stems. The wireless connection was unreliable, in particular, when the voltage level of the batteries was low. An average connection lasted about 4 min. □

5.4 Summation principle

Elementary motions add up to advanced movement – one benefit of using matrices. For instance, the front joint can bend while the robot turns. Moreover, wheel walking is superimposed at arbitrary rates to conventional forward driving and turning. The flexibility contributes to the overall performance in the field.

Figure 5.5: Assignment of joystick axes and buttons.

Remark 5.7. The joystick is an invaluable tool to manually operate Marsokhod, Figure 5.5. Since the robot has 8 motors, the design of a powerful yet convenient user interface is challenging. We distribute the functionality in the following way:

The left regulator adjusts the rate of straight driving and spinning v_1^{d}, and v_2^{d}. The right regulator enters the wheel walking loop in forward and backward direction with variable speed. The regulator also sets v_4^{d} to trench the soil with the front-right wheel.

The wheel walking mode is selected by pressing one of the four directions on the point-of-view field.

The 4 buttons in the front extend and contract the front and rear joints by contributing to v_6^{d}, v_7^{d}. During normal operation, the wheels compensate the bending of the joint with a value ρ as described in Remark 5.5.

One outlying button enables calibration mode to carry out Procedure 4.3. During calibration mode, only the joint motors are assigned a small duty cycle, based on the 4 buttons in the front. Calibration is only required once at the beginning. □

The subsequent derivation ensures that the resulting wheel velocities are feasible for all motors. Starting point is the linear combination of the matrices as

$$\hat{w} = \sum_{j \in J} m_j v_j + n_6 w_6 + n_7 w_7 \tag{5.4}$$

with coefficients $v_j \in \mathbb{R}$ for $j \in J$ under the constraint

$$|\hat{w}_i| \leq \zeta_i V_{\mathsf{icr}}(D) \frac{U}{\bar{\mathbf{U}}} \tag{5.5}$$

for all motors $i = 0, 1, \ldots, 7$, and a maximum duty cycle of $D \in (0, 1]$. The duty cycles assigned shall be feasible: The constraint guarantees $|d_i| \leq D$ for all motors.

We assume that the contribution of wheel walking satisfies the constraint (5.5), i.e.

$$|m_6 v_6 + n_6 w_6 + m_7 v_7 + n_7 w_7| \leq \zeta V_{\mathsf{icr}}(D) \frac{U}{\bar{\mathbf{U}}} \tag{5.6}$$

If any motor velocity $\hat{w}$ in (5.4) violates (5.5), we solve for the largest $\kappa \geq 0$ so that

$$\hat{w} = \kappa \sum_{j=1}^{3} m_j v_j + m_6 v_6 + n_6 w_6 + m_7 v_7 + n_7 w_7$$

satisfies the constraint (5.5).

The problem is equivalent to maximize $\kappa \geq 0$ among a set of equations of the form $|a\kappa + b| \leq c$ for numbers $a, b, c \in \mathbb{R}$ with $a \neq 0$ and $|b| \leq c$, which corresponds to assumption (5.6). The solution is

$$\kappa = \begin{cases} (c - |b|)/|a| & \text{if } \operatorname{sgn} a = \operatorname{sgn} b \\ (c + |b|)/|a| & \text{otherwise} \end{cases}$$

The linear combination $m_1 v_1 + m_2 v_2$ drives Marsokhod on a circle with radius proportional to $\frac{v_1}{v_2}$ for $v_2 \neq 0$. In case $v_2 = 0$, Marsokhod does not change orientation at all and drives on a straight line.

Chapter 6

Autonomous Reconfiguration

We fuse the results from the previous chapters to yield a driving support system. We offer a simple driving interface for operator control, and future application software. Our control software selects internal parameters based on the guidelines: safety of the mechanical structure and electronic appliances, stable operation, performance enhancement, and economies in energy.

When battery powered, the supply voltage drops considerably while the robot is in motion. Our software prevents the voltage to fall below a certain threshold, and thus improves operational stability, Section 6.1.

Marsokhod is designed to maneuvre on rough and inclined terrain. While the robot drives on a slope, our software ensures an increased ground base. However, when the robot is commanded to turn, the exterior axles are contracted. The values ρ_f, ρ_r are modified during wheel walking when load indicates that the joint does not move the exterior axle.

Depending on the ground conditions, the traction of the wheels might vary. Based on the perceived load, we shift power from slipping wheels to wheels with better grip. The redistribution makes Marsokhod appear more powerful and advance quicker. However, the robot deviates from the intended direction more easily.

6.1 Power management

When Marsokhod is powered by batteries, we intend to prevent a voltage drop exceeding a threshold $\Upsilon \geq \mathbf{U} - U$. For instance, $\Upsilon = 1.5$ V. This measure enhances driving safety and operational stability in the field. We achieve our aim by selecting a proper value D in (5.4), using the experimental results of Section 4.2.

As introduced in Section 5.4, D is the upper bound $\max |d_i| \leq D$ to the duty cycles assigned to the motors. Then, equation (4.5) simplifies to $\Upsilon = 8\xi D + \Xi L$, where the sum of the load squares $L := \sum_{i=0}^{7} l_i^2$ is known from the most recent measurements. We are

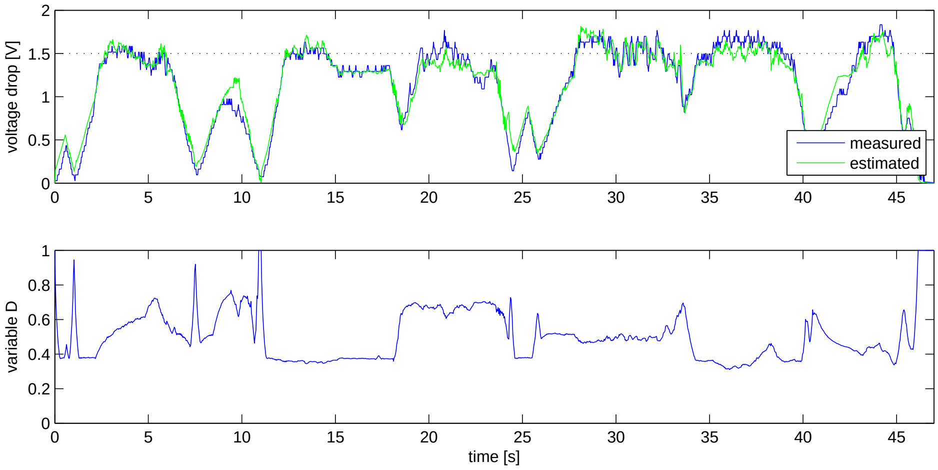

Figure 6.1: In the run of about 45 seconds, the power management ensures that the voltage drop does not exceed $\Upsilon = 1.5$ V.

interested in the solution

$$D(L) = \frac{1}{8} \frac{\Upsilon - \Xi L}{\xi} \tag{6.1}$$

Example 6.1. We omit the physical units for clarity. The voltage drop shall not exceed $\Upsilon = 1.5$ V at any time during operation. Using the batteries 2×HYS1250, we set $\xi = 0.6$, and $\Xi = 0.4$ refering to Section 4.2. Then, we yield $D(0) = 0.417$, $D(0.2) = 0.4$, $D(0.5) = 0.375$, $D(1) = 0.333$, and $D(2) = 0.25$ for a selection of values L. □

The expression (6.1) is a lower bound, which we refine to

$$D(L) = \min\left(\frac{\max |d_i|}{\sum_{i=0}^{7} |d_i|} \frac{\Upsilon - \Xi L}{\xi}, 1\right) \tag{6.2}$$

if $d_i \neq 0$ for some motor $i = 0, 1, \ldots, 7$, otherwise we set $D(L) = 1$. The factor that substitutes $1/8$ takes into account that commonly not all of the motors are assigned the absolute duty cycle D simultaneously.

We recapitulate the preceding derivations: To prevent a voltage drop beyond Υ, we define the upper bound to the duty cycles in (5.5) as

$$D^{k+1} = \min\left(\frac{\max_i |d_i^k|}{\sum_i |d_i^k|} \cdot \frac{\Upsilon - \Xi \sum_i (l_i^k)^2}{\xi}, 1\right) \tag{6.3}$$

if $d_i \neq 0$ for some motor $i = 0, 1, \ldots, 7$, otherwise we set $D^{k+1} = 1$.

Figure 6.1 plots the performance of the measure during a rough driving sequence. Filtering of the sequence D^k is unnecessary.

Field Experiment 6.2 (18. Jul 2008)**.** The experiment evaluated the power management. Besides, we emulated broken wheels. To improve the wireless communication, we mounted the link adapter on a mast, see Figure 6.2.

Figure 6.2: Left: Front-wheel walking. Center: Emulation of broken wheels cause faults in the sand. Right: Laptop with application software and joystick for operator control.

We report on the effects of broken wheels: With a rigid front wheel, driving forward was barely possible. During wheel walking, the exterior axle was immobile. A rigid wheel of the center axle made turning less efficient.

The displacement of the antenna and the power management made the communication more reliable. The computer rebooted when the voltage dropped to $U = 19.5$ V. At that point, the batteries did not supply sufficient current to the computer. □

6.2 Behaviour of joints

We develop autonomous reconfiguration of the joints based on the evidence of the accelerometer, the optical encoders, and also the driving parameters. According to our premise 'economies in energy', the joints shall only move when necessary.

The parameters that determine the control of the joint are

VAR	DESCRIPTION	BEHAVIOUR	SECTION
p_{min}	lower bound of inclination	prevent jack-knifing	6.2.1
p_{max}	upper bound of inclination	prevent jack-knifing	6.2.1
v_{d}	target velocity of joint	contract joint when robot spins	6.2.2
ρ	placement of exterior axle	axle stationary when load is high	6.2.3

The values p_{min}, p_{max}, and v_{d} impact (4.16), while ρ appears in (5.1) and (5.2). The behaviours might oppose the active control by the operator or the application software. However, the parameters change in a continous fashion, so that no jerky motion occurs. We outline the superposition of the behaviours:

At the begin of every iteration, we reset p_{min}, p_{max} to the values specified in (5.3). The bounds are then truncated based on the slant of the terrain.

The target velocity of the joint v_{d} is typically determined by the operator, for instance during the process of wheel walking. When Marsokhod is commanded to spin, however, the behaviour contributes to v_d based on the rate of rotation. While turning, the joints typically contract to reduce the wheel base.

The rolking mode determines the parameter $\rho \in [0,1]$. The load on the joint indicates if the exterior axle cannot be moved further. Then, the value ρ is autonomously modified to keep the axle stationary in order to prevent harm to the robot and the environment.

6.2.1 Slant response

When Marsokhod is located on a slope, we extend the joint that faces the downhill direction. The measure increases stability, improves the weight distribution, and reduces the mechanical load on the joint facing downhill.

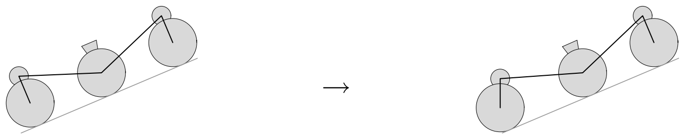
(6.4)

From the accelerometer readings a_acc we estimate the direction of gravity $g = (g_1, g_2, g_3)$ in the coordinate system of the sensor as

$$g^k = \frac{\bar{g}^k}{||\bar{g}^k||} \qquad \text{where} \qquad \bar{g}^k = \lambda g^{k-1} + (1-\lambda)\frac{a^k_\mathsf{acc}}{||a^k_\mathsf{acc}||}$$

for a coefficient λ close to 1, and $g^0 = (0,0,-1)$. Then, we approximate the inclination of the terrain σ along the coordinate axis x_1 of the robot as

$$\sigma = \arccos g_1 - \frac{\pi}{2} + \frac{\alpha_r - \alpha_f}{2}$$

The angle γ in the triangle

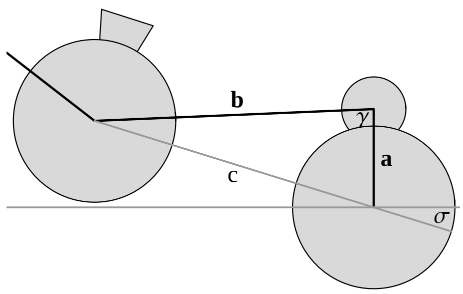

satisfies the relation $\mathbf{a} - \mathbf{b}\cos\gamma = -c\sin\sigma$ where $c = \sqrt{\mathbf{a}^2 + \mathbf{b}^2 - 2\mathbf{ab}\cos\gamma}$. The joint is parallel to the direction of gravity g when

$$\gamma(\sigma) = \arccos -\frac{1}{\mathbf{b}}\left(\mathbf{a}\mathrm{s} + \sqrt{(\mathbf{a}^2\mathrm{s} + \mathbf{b}^2)\sin^2\sigma}\right)$$

where $\mathrm{s} = -1 + \sin^2\sigma$.

Based on the slope of the terrain, we define

$$\begin{array}{lll} p_6^{\max} = -\arccos \mathbf{a}/\mathbf{b}, & p_7^{\min} = \gamma(\sigma) & \text{if } 0 \leq \sigma \\ p_6^{\max} = -\gamma(\sigma), & p_7^{\min} = \arccos \mathbf{a}/\mathbf{b} & \text{if } 0 > \sigma \end{array}$$

If the joint inclination violates $p_{\min} \leq p \leq p_{\max}$ as indicated in the lhs. of (6.4), the control (4.16) readjusts the joint back into the feasible region.

6.2.2 Contract arms when turning

With the limits $p_i^{\min}$, $p_i^{\max}$ for $i = 6, 7$ specified in (5.3), the wheel base ranges from 0.387 to 0.537 m. According to Procedure 5.1, the turning efficiency increases when the wheel base is reduced.

Our objective is to contract the joints when Marsokhod is intended to turn. We modify the existing target velocities of the joints v_6^{d}, and v_7^{d} to

$$\begin{aligned} v_6^{\mathrm{d}} &:= \operatorname{clip}\left(-\bar{v}_6, v_6^{\mathrm{d}} + |v_2^{\mathrm{d}}|, \bar{v}_6\right) \\ v_7^{\mathrm{d}} &:= \operatorname{clip}\left(-\bar{v}_7, v_7^{\mathrm{d}} - |v_2^{\mathrm{d}}|, \bar{v}_7\right) \end{aligned}$$

where $\bar{v}_6 = \mathbf{w}/\max|n_6|$, $\bar{v}_7 = \mathbf{w}/\max|n_7|$, and $\operatorname{clip}(a, b, c) := \min(\max(a, b), c)$. These bounds ensure that the bending of the joints are accompanied by feasible wheel velocities.

When Marsokhod drives uphill, i.e. $\sigma > 0$, we set $p_7^{\min} = \gamma(\sigma)$. In case the robot descends a slope, then $\sigma < 0$ and we set $p_6^{\max} = -\gamma(\sigma)$.

6.2.3 Placement of axle

During the process of wheel walking, obstacles might prevent the joint from bending in combination with the value ρ, that determines the placement of the joint axle.

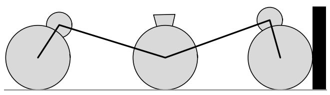

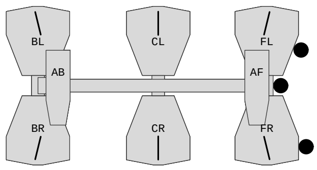

In the illustration, the front axle cannot advance. The front joint does not bend with $\rho_f = 1$ to advance the front axle. The rear joint does not bend with $\rho_r = 0$ to advance both axles, the center and front.

High load l_6, l_7 on the joint motor indicates that the robot should not advance further towards the obstacle. Due to the presence of the hindrance, the joint velocity v_6, v_7 is typically low in this moment. Thus, switching ρ_f to $1 - \rho_f$ does not create a discontinuity in the sum (5.4). Analogous, ρ_r is switched to $1 - \rho_r$. In case the joint velocities exceed a certain threshold, ρ_f and ρ_r are modified gradually.

Figure 6.3: Marsokhod climbing over a collection of obstacles arranged on a sandy slope.

The thresholds for the load, as well as for the joint velocity are chosen based on experiments and have been approved in the field. Quote 2.1 by the engineers of Marsokhod urges us to conduct

Field Experiment 6.3. [22. Jul 2008] We navigated Marsokhod in a course full of obstacles, see Figure 6.3. The objective was to investigate the benefit of adjusting the axle clearance:

The bending of the joints was useful to position individual axles with respect to the obstacles. Wheel walking helped to advance the robot, while at least one axle had solid grip.

We excavated a 9 cm layer of sand by rotating the front-right wheel slowly. The automated driving support resulted in stable operation.

To prolong the duration of the run, we switched to tether-fed supply after the first pair of batteries had depleted. The display at the power supply revealed that the current flow might exceed 5 A. Driving in extreme configurations involved to extend some of the cables between the center unit and the ReadyBoard. □

Field Experiment 6.4. [23. Jul 2008] We navigated Marsokhod on the same course as in Field Experiment 6.3. One objective was test the new wires.

The robot was powered through a tether, which created a relaxed testing environment. Two pairs of batteries were installed as payload only.

The operator improved his skills in the handling of the robot, see Remark 5.7. The placement of the axles was achieved with more confidence than in the previous test.

The wireless communication stabilized after a few interruptions at the beginning. □

6.3 Load distribution

In the field experiments, several driving situations occur frequently:

	SITUATION	DESIRED BEHAVIOR
a)	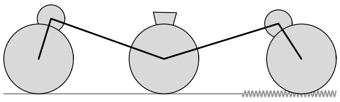	wheels on slippery ground slow down, while wheels with traction speed up
b)	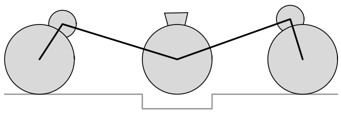	wheels without contact are stopped, while wheels with traction speed up
c)	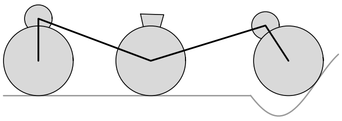	faster wheels speed up, while wheels with load slow down

Our goal is that Marsokhod approaches the desired behavior to enhance the performance. While the robot is commanded to drive straight, i.e. $v_1 \neq 0$, we add a correction term $h(l)$ to the wheel control $\hat{w}$ that is based on the instantaneous load.

We experiment with two terms h^{v}, and h^{s}. In the formulas, we utilize the mean load $\bar{l} = \mathrm{mean}_i l_i = \frac{1}{6}\sum_{i=0}^{5} l_i$ on the six wheels and the variance $\mathrm{var}(l) = \frac{1}{5}\sum_{i=0}^{5}(l_i - \bar{l})^2$.

We define

$$h_i^{\mathrm{v}}(l) = \mathrm{clip}\left(-H, \frac{5}{\mathrm{rad/s}}(\bar{l} - l_i)\sqrt{\mathrm{var}(l)}, H\right) \tag{6.5}$$

as well as

$$h_i^{\mathrm{s}}(l) = \mathrm{clip}\left(-H, \frac{5}{\mathrm{rad/s}}[\mathrm{mean}_j\left((\bar{l} - l_j)l_j\right) - (\bar{l} - l_i)l_i]\,\mathrm{sgn}\, v_1, H\right) \tag{6.6}$$

where $\mathrm{clip}\,(a, b, c) := \min(\max(a, b), c)$. Both terms satisfy $\sum_i h_i^{\mathrm{v}} = \sum_i h_i^{\mathrm{s}} = 0$, which implies that the final control $\hat{w} + h^{\mathrm{v}}$, and $\hat{w} + h^{\mathrm{s}}$ are simply a redistribution of the original $\hat{w}$. Since no load velocity and duty cycle relate almost linearly, the sum of the absolute duty cycles $\sum_i |d_i|$ remains vaguely constant. According to Remark 4.12, we expect the current consumption to rise in the situations a), and b). The constant of 5 is selected based on experience. To ensure stability, we clip the values at H. Usually, $H = 0.3$ rad/s is a good choice.

Example 6.5. We display the performance of the correction terms (6.5) and (6.6).

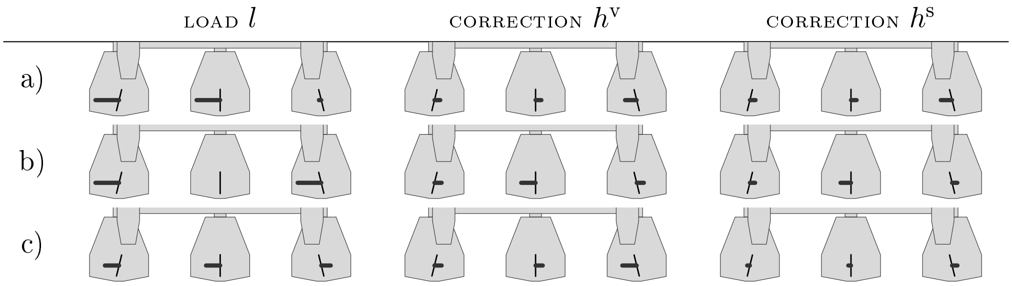

The term h^{s} approaches the desired behavior in all three situations. The correction h^{v} fails to speed up the wheel with excess velocity. However, the behaviour is least important in the field. $\square$

The control with load distribution $\hat{w} + h^{\mathrm{v}}$ as well as $\hat{w} + h^{\mathrm{s}}$ where tested and approved in

Field Experiment 6.6. [25. Jul 2008] We drove Marsokhod outside on heterogeneous terrain: sand, gravelstone, bricks, slices of tree trunks, and styrofoam. The obstacles were arranged along a slope. The objective of the test was to experience the driving resulting from the load distribution h^{v}, as well as h^{s}.

The operation was stable; oscillations did not occur. At low values of v_1, Marsokhod appeared to be more powerful and to advance quicker. However, the robot deviated from the intended direction more easily. Also, Marsokhod tended to scratch over the bricks.

Besides, we compared different wheel walking modes with plain driving when moving uphill on sand: Wheel walking caused significantly less erosion. $\square$

Field Experiment 6.7. [29. Jul 2008] At this point, the software was finalized. The objective of the field experiment was to test the demo application software, and to make an instructive video recording that illustrates the use of the joystick.

The driving support was activated and facilitated the handling of the robot.

Both, the high- and low-level control algorithms ran on the onboard computer of the robot, while the demo application downlinked the state of the joystick via wireless communication, see Illustration 3.9. A temporary communication blackout of more than 0.5 s would cause the software on the ReadyBoard to safely stop the motors. During the 30 min of operation, however, no interruptions occured. $\square$

Conclusion

Working with Marsokhod is enjoyable and rewarding. The numerous field experiments demonstrate the reliability of the hardware that we have modified, and the software that we have developed. The few problems that we encountered and their solutions list as

PROBLEM	POSSIBLE SOLUTION
wireless connection fails	check status with `ifconfig` command, use correct IP address, reboot ReadyBoard with wireless adapter plugged in
one or more chips do not respond via CAN communication	cut the power to the chips, tighten connectors at the power distribution board, then resupply chips
joints bend incorrectly	perform Procedure 4.3 for calibration
inappropriate slant response	adjust inclination of accelerometer sensor with the robot on flat terrain until the LCD reads ≈ 0 deg.

Our efforts and results enable researchers to smoothly drive Marsokhod, control the inclination of the joints, and access the sensor measurements. A compact demonstration of operator control using a joystick is included in the software, see Figure 8.1. We refrained from enforcing wheel velocities. The motors are extremely powerful and might harm the robot or the environment. We caution the operator not to drive the robot at maximum speed.

The odometry of Marsokhod is meaningless when driving on granular soil, in particular, when the robot is turning. Reliable localization in a global context is a key feature to more autonomy. In one of the field experiments, we tested visual odometry using a mono camera. The dynamic shadows as well as the jerky contact on rough terrain prohibited a consistent positioning. Since Marsokhod is operated in the open country, we suggest to install a 3d-laser scanner. The precise awareness of the obstacles should help to appropriately adjust the clearance of the axles by bending the joints.

The protective covers that we manufactured for the wheels allow to drive Marsokhod on the floor inside. Since the laboratory has several mobile robots, we envision Marsokhod being part of a multi-robot arrangement.

Theses

Let us accentuate the major contributions of this thesis.

- We model the backlash in the joints using the piecewise linear functions P and $P^{\pm}$ in order to bend the joints smoothly.
- The motors are calibrated individually. Equation (4.3) correlates the duty cycle d to the no load speed $\hat{w}$. With the help of the transfer function δ, we measure the instantaneous load l. We approximate the voltage drop as a linear combination of the absolute duty cycle $|d|$ and the load squared l^2 in (4.5).
- The difference in measured velocity w and no load velocity ν is proportional to the external torque τ on the wheel as expressed by (4.7).
- The position and velocity control presented in Lemma 4.15 is elaborated and versatile. The control is suitable for bending the joints. The velocity control is used to accelerate the robot smoothly when driving straight and turning.
- The mobility of Marsokhod is spanned by the elementary motions $m_1, m_2, \ldots, m_7$. Section 5.4 discusses how to scale the components to obtain a feasible maneuvre.
- When turning Marsokhod, the wheels of the center axle should not slip, but bear as much load as possible. The wheels of the front and rear axles are required to move faster by a factor $F(c_f)$, and $F(c_r)$.
- Despite the inclined blades on the wheels, Marsokhod is not able to drift sidewards.
- We present the most common modes of wheel walking and explain how to control any of the modes manually using only 4 buttons of a joystick.
- By manipulating the scaling of the elementary motions, we prevent a voltage drop greater than a certain value Υ. The behavior enhances the stability of operation in the field.
- When driving on a slope, the joint that faces downhill is extended autonomously. Turning contracts the joints to provide a more compact wheel base. The joints do not bend against obstacles with all force, but the robot backs up to facilitate the bending.
- We shift power from slipping wheels to wheels with better grip based on the perceived load l. The redistributions $h^{\mathrm{v}}, h^{\mathrm{s}}$ make Marsokhod appear more powerful and advance with less erosion of the soil.

Bibliography

[AA98] G. Andrade, F. Amar, P. Bidaud, R. Chatila: *Modeling Robot-Soil Interaction for Planetary Rover Motion Control*, International Conference on Intelligent Robots and Systems, Proceedings, 1998

[At08] Atmel: *8-bit AVR Mircocontroller with 32K/64K/128K Bytes of ISP Flash and CAN Controller*, Datasheet, Revision C, 2008

[CW97] D. Christian, D. Wettergreen, M. Bualat, K. Schwehr, D. Tucker, E. Zbinden: *Field Experiments with the Ames Marsokhod Rover*, Proceedings of the 1997 Field and Service Robotics Conference, 1997

[Di06] R. Dickmann: *Das Kappen der historisch-systematischen Taue einer Verfassungsnorm - Eine kritische Betrachtung der Entscheidung des Bundesverfassungsgerichts zur Bundestagsauflösung 2005*, Bayerische Verwaltungsblätter (BayVBl.) 2006, S. 72–75

[El07] M. Elsdörfer: *Ein tiefer Blick in "leere" Schubladen - Deutsches im Nachkriegstheater 1945-1948*, Verlag Peter Lang, 2007

[Gr07] J. Groeger: *Twistor Spinors in Signatures* $(1, n-1)$ *and* $(2, 2)$, Diploma Thesis, Humboldt Universität zu Berlin, 2007

[Ha04] J. Hakenberg: *Interactive World Simulation*, 2004, `www.hakenberg.de/graphics/world.htm`

[Ha08] J. Hakenberg: *Mobility and Autonomous Reconfiguration of Marsokhod, software and video material*, 2008, `www.hakenberg.de/automation/marsokhod.htm`

[Ke90] A. Kermurjian: *From the Moon Rover to the Mars Rover*, reprinted from the July/August 1990 issue of The Planetary Report, `www.planetary.org/programs/projects/space_information/tpr_1990_4_kermurjian.html`

[Ke07] M. Kena: *Analysis and Application of Subdivision Surfaces*, Master's Thesis, Department of Production and Metallurgy Engineering, University of Technology Baghdad, 2007

[KG92] A. Kemurdjian, V. Gromov, V. Mishkinyuk, V. Kucherenko, P. Sologub: *Small Marsokhod Configuration*, IEEE International Conference on Robotics and Automation, Proceedings, 1992

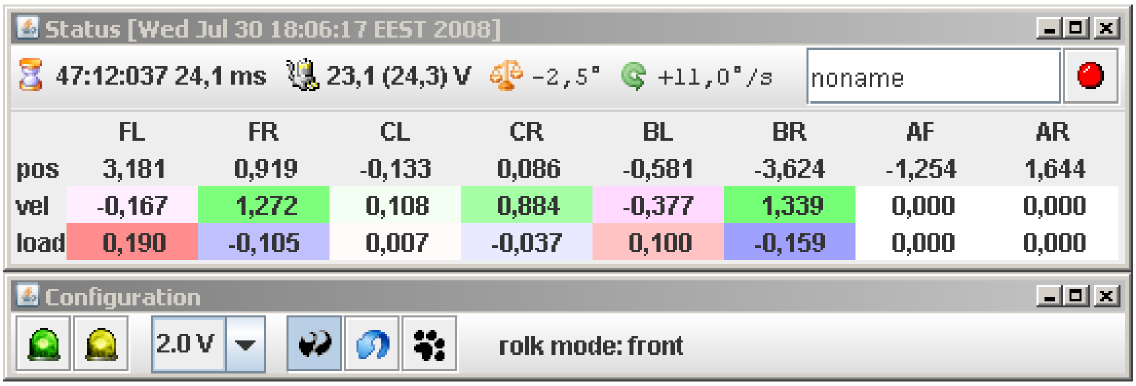

Figure 8.1: User interface of the demo program.

[La08] S. Lacroix: *The marsokhod rover Lama*, Robotics in Natural Environments, LAAS/CNRS, `www.laas.fr/~simon/eden/robots/lama.php`

[Le07] I. Leppänen: *Automatic locomotion mode control of wheel-legged robots*, Series A: Research Reports No. 30, Automation Technology Laboratory, Helsinki University of Technology, 2007

[LS07] LSI Computer Systems, Inc.: *LS7183–LS7184, Quadrature Clock Converter*, USA, 2007

[PL03] T. Peynot, S. Lacroix: *Enhanced Locomotion Control for a Planetary Rover*, International Conference on Intelligent Robots and Systems, Proceedings, 2003

[Po07] Port: *can4linux – CAN network device driver*, 2007, `www.port.de/software/can4linux/`

[Sc07] I. Scholz: *Analysis of HIV-1 gag matrix and capsid domain mutations and their effects on virus assembly and infectivity*, Dissertation, Oregon Health and Sciences University, 2007

[SC01] C. Stoker, N. Cabrol: *The 1999 Marsokhod rover mission simulation at Silver Lake, California: Mission overview, data sets, and summary of results*, Journal of geophysical research, vol. 106, pp. 7639–7663, 2001

[TK08] Helsinki University of Technology: Faculty of Electronics, Communications and Automation, Department of Automation and Systems Technology `www.automation.tkk.fi/`

[Za96] A. Zakharov: *Robotic spacecraft mission to mars*, Space Research Institute, 1996 `www.iki.rssi.ru/mars96/`